Chapter 3

Proteome consequences of *P. falciparum* AdoMetDC inhibition with MDL73811

3.1 Introduction

The proteome is more complex than the genome, since a single gene can give rise to several protein isoforms, and therefore proteomics tries to directly determine the level of gene products present in a cell, usually in the form of proteins (Ong & Mann, 2005). Biological processes are mainly controlled by proteins and their interacting partners which will determine the protein function. Many factors apart from mRNA abundance determine the protein levels and include PTM's and mRNA decay mechanisms (Ong & Mann, 2005), therefore increasing the complexity of the proteome. Various protein isoforms can be created all with different functions within the cell. PTM's are the chemical reactions by which a newly synthesised polypeptide is converted into a functional protein either by addition of a chemical group or by proteolytic cleavage (Canas *et al.*, 2006). It is considered that the goals of protein expression profiling is to increase identification and quantification of components that are unique to a particular life stage or of a particular diseased state (Johnson *et al.*, 2004). This property therefore makes proteomics ideal to study the life stages of the Plasmodial parasites as well as the response of the parasite to a specific perturbation.

3.1.1 Plasmodial perturbation studies investigated by proteomics

The first Plasmodial proteomic study was a large scale high accuracy mass spectrometric analyses of various Plasmodial life stages (Lasonder *et al.*, 2002). A total of 1289 proteins were identified of which 714 were related to the asexual blood stages of mainly trophozoites and schizonts. A further 931 proteins were identified that were related to gametocytes and 645 proteins related to gametes. Of the 1289 proteins identified between all the life stages, it was determined that a total of 350 proteins were shared between all 3 stages investigated (Lasonder *et al.*, 2002). Another large scale proteome investigation was done using multidimensional protein identification technology (MudPIT) (Florens *et al.*, 2002). A total of 2415 parasite proteins were identified that related to the trophozoite, merozoite, sporozoite and gametocyte proteome of *P. falciparum* strain 3D7. Of these, only 152 (6%) proteins were shared between all 4 stages, indicative of stage-specific protein production (Florens et al., 2002).

The first 2-DE proteomic study established a 2-DE protocol for quantitative protein determination by the incorporation of heavy and light isoleucine into the media and therefore into the proteins under investigation (Nirmalan *et al.*, 2004a). The isoleucine labelled proteins can then be identified and quantified by mass spectrometry (MS). The protein abundance of selected proteins under PYR pressure was also investigated (Nirmalan *et al.*, 2004a). Two-dimensional gel electrophoresis has subsequently been used to determine the differences between 4 *P. falciparum* laboratory strains using metabolic labelling (Wu & Craig, 2006). Possible differences in cyto-adherence between the strains were determined and can be exploited for possible future drug development (Wu & Craig, 2006). The effect of the active ingredients in CoArtem (artemether and lumefantrine) was also investigated by 2-DE (Makanga *et al.*, 2005). Drug-specific effects were determined for both lumefantrine and artemether, which was associated with an increased protein abundance of specific proteins under drug pressure from one compound but the opposite effect with the other compound (Makanga et al., 2005). Parasites challenged with an endoperoxide-containing compound was investigated by 2-DE and revealed the increased protein abundance of 12 protein spots and decreased protein abundance of 14 protein spots of which only 15 protein spots were from Plasmodial origin (Aly *et al.*, 2007).

The mode-of-action of CQ was investigated by the use of 2-DE (Radfar *et al.*, 2008). The oxidised protein status of proteins was determined since it was hypothesised that CQ produces oxidative stress within the parasite. A total of 79 protein spots were identified which represented 41 unique proteins (Radfar et al., 2008). The mode-of-action of CQ was also investigated on CQ-resistant and CQ-sensitive strains using surface enhanced laser desorption ionisation-time of flight (SELDI-TOF) MS analysis (Koncarevic *et al.*, 2007). Hierarchical clustering of the data revealed clear patterns associated with CQ-sensitive and CQ-resistant strains, therefore revealing vital information on the mode of resistance to chloroquine. Further analysis revealed 10 possible CQ-resistance markers (Koncarevic *et al.*, 2007). In another CQ based study, the effect of CQ and artemisinin on Plasmodial parasites were determined using isoleucine-based SILAC in combination with MudPIT (Prieto *et al.*, 2008). The proteome of CQ treated parasites revealed oxidative proteins while artemisinin did reveal changes in the ATP vacuolar synthase subunits. Interestingly, the multiple drug resistant protein *(Pfmdr1)* was up-regulated in both CQ and artemisinin treatment reiterating its involvement in parasite resistance (Prieto *et al.*, 2008). Forty-one proteins were up-regulated, while 14 proteins were down-regulated with CQ treatment and 38 proteins were up-regulated and 8 were down-regulated with artemisinin treatment.

3.1.2 Perturbation of polyamine metabolism on the proteome

Co-inhibition of AdoMetDC/ODC in *P. falciparum* resulted in the identification of 6 differentially affected proteins (van Brummelen *et al.*, 2009). Of these, S-adenosylmethionine synthase (AdoMet synthase) had decreased protein abundance, while the protein abundance of ornithine aminotransferase (OAT) and pyridoxal-5'-phosphate (PLP) synthase increased. These polyamine specific proteins reveal some compensatory mechanisms. The regulation of ornithine may be a compensatory effect in order to homeostatically control the levels of ornithine that may be toxic to the parasite in high levels, while the decreased protein abundance of AdoMet synthase may be an attempt to maintain AdoMet levels within the parasite (van Brummelen et al., 2009). This study was followed by the determination of the proteome of cyclohexylamine inhibited spermidine synthase (Becker *et al.*, 2010). This investigation revealed the differential regulation of 38 spots over 3 time points of which 21 protein spots could be identified by MS. Four of the identified proteins were related to polyamine metabolism and included OAT (PFF0435w), AdoMet synthase (PFI1090w), purine nucleoside phosphorylase (PNP)(PFE0660c) and adenosine deaminase (PF10_0289), all of which were down-regulated (Becker et al., 2010).

This chapter investigates the proteome of *P. falciparum* AdoMetDC inhibited with MDL73811 with the 2-DE approach that was established in Chapter 2. The proteome was first investigated by SDS-PAGE in which 29 unique Plasmodial protein groups were identified by LC-MS/MS. This was followed by the determination of the proteome of MDL73811 inhibited parasites by 2-DE in which 91 protein spots were identified which accounts for 46 unique Plasmodial protein groups that were identified at two time points, and included the differential regulation of several polyamine-related proteins.

3.2 Methods

3.2.1 Malaria SYBR Green I-based fluorescence (MSF) assay for IC_{50} determination

The SYBR green assay was developed to be easy to use, cheap, and have robust performance and speed (Smilkstein *et al.*, 2004). The assay is based on the principle that the dye binds to DNA and since erythrocytes do not contain DNA or RNA only the parasite DNA will be stained (Bennett *et al.*, 2004). The SYBR Green dye has a very strong affinity for DNA and once bound to the DNA will fluoresce (Bennett et al., 2004, Smilkstein et al., 2004). Parasite cultures were centrifuged at 3000×*g* for 5 min to obtain a pellet that will be used for experimental procedures. First, the parasitemia was determined by counting parasites on Giemsa stained thin smears in at least 10 different microscopic fields containing about 100 erythrocytes each (10×100). The cultures were then diluted to 1% parasitemia and 2% hematocrit in culture media. A sterile 96-well plate was used for the assays to follow. The first column of the plate was filled with only culture media (300 µl) and not used as part of the IC_{50} determination due to the possibility of edge effects. The second column contained 0.5 µM CQ as a negative control (300 µl), and represented total inhibition of parasite and hence no parasite growth. This was followed by the positive control that contained parasites in drug-free media (300 µl). The next 8 columns contained a serial dilution of the drug starting at the highest concentration of 16 µM MDL73811 (in PBS) to the lowest concentration of 0.125 µM MDL73811. The plate was then placed into a gas chamber and gassed for 2 min, before being placed in a 37ºC incubator for 96 h. On the day of the assay, SYBR green buffer was prepared by adding 2 µl of SYBR green (Invitrogen) in 10 ml lysis buffer (20 mM Tris, pH 7.5; 5 mM EDTA; 0.008 % (w/v) saponin; 0.08 % (v/v) Triton X-100) and kept in the dark. One hundred microlitres of the SYBR green lysis buffer was pipetted into each of the wells of a 96-well black fluorescence plate (Nunc) followed by 100 µl of resuspended, treated parasites. The plate was then incubated for 1 h in the dark at room temperature before the fluorescence was measured using the Fluoroskan Acent FL Fluorimeter (Thermo LabSystems) at excitation of 485 nm and emission at 538 nm (integration time of 1000 ms). Data were analysed using SigmaPlot 9.0 to determine the IC_{50} of MDL73811 against *Pf*3D7.

3.2.2 Morphology study

To determine the morphological time of parasite arrest induced by the drug MDL73811, a morphological study was done using Giemsa stained blood smears as described earlier (Section 2.2.3). MDL73811 was dissolved in PBS, and filtered using a 0.22 µm Ministart syringe filter.

Aliquots were stored at -20°C until use. Parasites were treated with 10 µM MDL73811 (10×IC_{50}) just before or during invasion. A similar amount of PBS was added to the control parasite cultures to eliminate any possible effect of PBS on the parasites. A blood smear was made every 2-5 h to morphologically follow the parasite during the intraerythrocytic cycle and was continued for a total of 60 h. Slides were analysed using a Nikon light microscope at 1000× magnification under oil immersion. At least 10 fields of 100 erythrocytes each were examined for the determination of parasite progression.

3.2.3 Culturing for the proteomic time study

*Pf*3D7 parasites were maintained *in vitro* in human O^+ erythrocytes in culture media as described in chapter 2 section 2.2.3. Parasites were monitored daily through light microscopy of Giemsa stained thin blood smears as described in section 2.2.3. Before treatment could commence the parasites were always synchronised for 3 consecutive cycles (6 times in total, always 8 h apart once in the morning and later in the afternoon) as described in section 2.2.4. A starting parasite culture (in the schizont stage) at 2% parasitemia, 5% hematocrit was treated with 10 µM MDL73811 at invasion after which the parasitemia increased to 10% in both the treated and untreated samples in the ring stage. A small scale morphology study was always conducted at the same time, and used as a positive control to ensure parasite arrest at ~26 h as the drug takes effect in the treated parasite culture. Sixty milliliters of *Pf*3D7 parasites at 10% parasitemia and 5% hematocrit were used per gel and harvested at 16 HPI (time point 1, t_1) and 20 HPI (t_2), and contained 4 biological replicates for each time point. 10% (w/v) Saponin was added to the infected erythrocytes to a final concentration of 0.01% (v/v), and incubated on ice for 5 min to lyse the erythrocytes and release the parasites. Parasites were collected by centrifugation at 2500×*g* for 15 min, and washed at least 4 times in 1 ml PBS at 16 000×*g* for 1 min until the supernatant was clear (Smit *et al.*, 2010). The parasite pellet was stored at –80°C until further use, but never stored for longer than 30 days.

3.2.4 Protein preparation

The 4 parasite pellets were pooled and then suspended in 500 µl lysis buffer as described by Nirmalan *et al.* (8 M urea, 2 M thiourea, 2% CHAPS, 0.5% (w/v) fresh DTT and 0.7% (v/v) ampholytes) (Nirmalan *et al.*, 2004a). Samples were pulsed-sonicated as described in section 2.2.6. Sonication was followed by centrifugation at 16 000×*g* for 60 min at 4°C, after which the protein-containing supernatant was used in subsequent 1-D SDS-PAGE and 2-DE and the remaining pellet was also used for 1-D SDS-PAGE (see following sections).

3.2.5 Protein quantification by 2-D Quant kit

The commercially available 2-D Quant Kit (GE Healthcare) was used according to the manufactures instructions with a few modifications as described in Chapter 2 section 2.2.7.4.

3.2.6 SDS-PAGE gels

Sixty micrograms of the supernatant containing proteins were dissolved in reducing buffer (0.06 M Tris-HCl, 2% (w/v) SDS, 0.1% (v/v) glycerol, 0.05% (v/v) β-mercaptoethanol and 0.025% (v/v) bromophenol blue, pH 6.8), boiled for 5 min before loading equal amounts of protein onto a 12.5% SDS-PAGE gel (Hoefer SE600, 16×18 cm). Similarly the pellet proteins were also dissolved in reducing buffer but were boiled for 10 min and vortexed vigorously to dissolve the pellet proteins before being loaded onto the 12.5% SDS-PAGE gels (Hoefer SE600, 16×18 cm). The gels were allowed to run until the bromophenol blue front reached the bottom of the gel. The gels were then removed from the glass plates and immersed in Colloidal Coomassie solution and left shaking overnight. The gels were rinsed with 25% methanol, 10% acetic acid before destaining with 25% methanol, until the background was clear (Neuhoff *et al.*, 1988). The gels were scanned on a Versadoc 3000 and analysed using the Quantity One 4.4.1.

3.2.7 1-DE SDS-PAGE spot identification by liquid chromatography electrospray ionization tandem mass spectrometry (LC-ESI-MS/MS)

The bands of interest were cut from each of the 4 SDS-PAGE gels, dried and stored at -20°C. Each gel piece was cut into smaller cubes and washed twice with water followed by 50% (v/v) acetonitrile for 10 min each. The acetonitrile was replaced with 50 mM NH_4HCO_3 and incubated for 10 min, repeated 3 times until the gel pieces was clear and free from CCB. The gel pieces were incubated in 100% acetonitrile until they turned white. This was followed by another NH_4HCO_3, acetonitrile wash step, after which the gel pieces were dried *in vacuo*. Gel pieces were digested with 10 ng/µl trypsin at 37°C overnight. Resulting peptides were extracted twice with 70% acetonitrile for 30 min, and then dried and stored at -20°C. Trypsin digested samples extracted from gel-plugs were re-suspended in 100 µl 0.5% acetonitrile, 0.5% formic acid and centrifuged at 16 000×*g*, 4°C for 15 min. Samples were analysed on an Agilent 1100 HPLC system equipped with capillary and nano-LC pumps coupled to a QSTAR ELITE mass spectrometer. Sample (1-2 µg) were de-salted on a Symmetry C18 trap column (0.18×23.5 mm) for 20 min at 20 µl/min using 0.5% acetonitrile/0.5% formic acid. Peptides were separated on a NanoEase XBridge C18 column (0.1×50 mm) connected to the trap column via 6-port switching valve. Peptide elution was achieved

using a flow-rate of 800 nl/min with a gradient: 0-10% B in 1 min, 10-30% B in 30 min, 30-50% B in 5 min, 50-100% B in 1 min; 100% B for 10 min (A: 2% acetonitrile, 0.5% formic acid; B: 98% acetonitrile, 0.5% formic acid). Nano-spray was achieved using a MicroIonSpray head assembled with a New Objective, PicoTip emitter (o.d. 360 µm; i.d. 75 µm; tip i.d. 15 µm). An electrospray voltage of 2.5-3.0 kV was applied to the emitter. The QSTAR ELITE mass spectrometer was operated in Information Dependant Acquisition (IDA) using an Exit Factor of 2.0 and Maximum Accumulation Time of 2.5 s. MS scans were acquired from m/z 400 to m/z 1600 and the 3 most intense ions were automatically fragmented in Q2 collision cells using Nitrogen as the collision gas. Collision energies were chosen automatically as function of m/z and charge. Protein identification was performed using the Paraghon™ algorithm *Thorough* search in Protein Pilot. An identification confidence of 95% was selected during searches with a False Discovery Rate (FDR) determined for the experiment.

3.2.8 Two-dimensional gel electrophoresis (2-DE) and staining

Four hundred micrograms of protein in rehydration buffer was applied to an 18 cm IPG, pH 3-10 L strip as described in section 2.2.9. First dimensional IEF commenced with a 10 h active rehydration step and followed an alternating gradient and step and hold protocol that was always allowed to proceed to a total of 35 000 Volt-hours, that completed within 17 h. The complete IEF focusing steps is given in Table 3.1.

Table 3.1: The IEF focusing steps used for 18cm IPG, pH 3-10 L strips.

Step	Voltage limit (V)	Time or Volt hour (h) or (V-h)	Gradient
1	30 V	10:00 h	Step and hold
2	200 V	0:10 h	Gradient
3	200 V	0:20 h	Step and hold
4	500 V	0:20 h	Gradient
5	500 V	0:20 h	Step and hold
6	2 000 V	0:20 h	Gradient
7	2 000 V	0:45 h	Step and hold
8	8 000 V	1:40 h	Gradient
9	8 000 V	24 000 V-h	Step and hold
Total		35 000 V-h	

IPG strips were equilibrated and placed on top of the 10% SDS-PAGE gel and covered with 1% agarose as described in section 2.2.9. Separation was performed at 80 V at 20°C until the bromophenol blue front reached the bottom of the gel. The gels were then fixed overnight in 40% (v/v) ethanol, 10% (v/v) acetic acid. After an overnight fixing step the gels were subsequently stained in 200 ml Flamingo Pink working solution and incubated with gentle agitation in the dark

for 24 h, to increase the sensitivity of the stain as described in section 2.2.10.1. All gels were stored in Flamingo Pink at 4°C until use for MS.

3.2.9 Image Analysis of 2-DE gels by PD Quest

PD Quest 7.1.1 was used to identify the number of spots on each of the 16 gels (4 untreated and 4 treated per time point) that were done for the 2 time points as was done in section 2.2.11. First, all images were cropped to the same dimensions (1.59 Mb, 933 × 893 pixels, 303.7 × 290.7 mm). The images were then filtered using the Filter Wizard, with the following settings that were manually incorporated by the user: the salt setting (light spots on dark background) was chosen since the fluorescent stain will show the spots as bright spots with a black background, outlier (chosen according to gaussian curve calculated by software) and filter size 3 × 3 was set to filter the image. The gel with the most spots and least streaks were then manually selected as the master image. Automated spot detection was performed by the Spot Detection Wizard and manually selecting a small spot, faint spot and large spot as the minimum and maximum spot selection criteria. The Spot Detection Wizard was also set to eliminate horizontal- and vertical streaking, subtract the background according to the floating ball method (automatically determined by the software), perform smoothing using a 3 × 3 filter according to the power mean filter type (suggested by the software). Additional settings for both t_1 and t_2 were manually selected for spot detection and are given in Table 3.2. After automatic matching of the 8 gels, every spot were manually verified to determine correctness of matching. Finally, reports were created to display information on the number of spots regulated for both time points.

Table 3.2: Spot selection criteria for the 2 time points

Settings	t_1	t_2
Scan area (mm)	366.0 × 336.7	308.6 × 293.3
Pixel size (µm)	390.6 × 390.6	325.5 × 325.5
Sensitivity	5.31	4.35
Size scale	5	5
Min peak	808	4712
Vertical radius	55	43
Horizontal radius	35	39
Large spot size	34 × 54	34 × 54
Floating ball radius	35	39
Smoothing	Power mean (3 × 3)	Power mean (3 × 3)

3.2.10 2-DE spot identification by tandem mass spectrometry

The spots of interest were cut from each of the gels and pooled, dried and stored at -20°C. The gel pieces were then prepared for MALDI-TOF MS/MS as described in section 2.2.12. The peak lists for each gel piece was then submitted to MASCOT as described in section 2.2.13.

3.2.11 Western blots

The protein containing lysates from the treated and untreated samples were quantitatively loaded onto a 12.5% SDS-PAGE gel with an initial voltage of 30 V for 30 min followed by 100 V until the bromophenol blue front had reached the bottom of the gel and electrophoresis was stopped. The gel was removed from the glass plates and then equilibrated for 5 min in 10 mM (3-(cyclohexylamino)-1-propanesulfonic acid (CAPS), pH 9.0. The membrane was cut to size and activated for 15 s in methanol and then placed in 10 mM CAPS to equilibrate.

Filter paper was equilibrated in 10 mM CAPS and then placed on a transfer cell. This was followed by the PVDF membrane and the gel placed on top of the membrane followed by another 5 layers of equilibrated filter paper. The blot proceeded for 45 min at 10 V. After blotting, the membrane was blocked overnight in blocking buffer (3% (w/v) BSA, 0.5% (v/v) Tween in PBS) at 4°C.

The gel was stained overnight in colloidal coomassie blue as described in chapter 2 section 2.2.10.4. This was done to ensure that complete transfer of all the proteins did occur. The next morning, the blocking buffer was removed and replaced with the primary antibody (1:4000) in wash buffer (1% (w/v) BSA, 0.5% (v/v) Tween in PBS) for 1 h at 37°C. This was followed by washing of the membrane with wash buffer for 10 min at 37°C, repeated 6 times. The membrane was then incubated with the secondary antibody (1:10 000) in wash buffer for 1 h at 37°C. Once again, this was followed by washing of the membrane and repeated 6 times. Finally, the membrane was incubated for 5 min with equal volumes (4 ml each) of Luminol/Enhancer solution (Pierce) and stable peroxidase solution (Supersignal West Pico Chemiluminescent substrate, Pierce). This works on the principle that the horseradish peroxidase enzyme that is conjugated to the antibody generates a hydroxide ion that gives rise to the transition of luminal to 3'-aminophthalate with the concurrent emission of light. The excess reagent was drained and then the membrane was exposed to Hyperfilm ECL X-ray film (Pierce) for 30 s in the dark. The X-ray were developed for 1 min in Universal Paper developer (Illford), rinsed briefly in water and then fixed for 3 min with Rapid Paper Fixer (Illford). The film was again rinsed in water and left to dry before being scanned on the Versadoc-3000 using Quantity One 4.4.1 (Bio-Rad), with the following settings: Densitometry, X-

ray film, Clear white TRANS, 0.5× Gain and 1×1 Bin. The density (ODu/mm^2) of each spot on the X-ray film was calculated using Quantity One and then the ratio of UT/T were calculated. The primary antibody for M1-family aminopeptidase (M1-AP) was a kind gift from Dr Isabelle Florent from Museum National d'Histoire Naturelle, Paris, France. The primary antibody for phosphoethanolamine N-methyltransferase (PEMT) was a kind gift from Prof Choukri Ben Mamoun from the Department of Genetics and Developmental Biology, University of Connecticut, USA.

3.3 Results

3.3.1 IC_{50} determination of MDL73811

Before a full scale proteomic investigation could be attempted, the IC_{50} of MDL73811 against the CQ sensitive *P. falciparum* parasite 3D7 strain (*Pf*3D7) had to be determined and was done using the Malaria SYBR Green I-based fluorescence (MSF) assay. A *Pf*3D7 parasite culture at 1% parasitemia, 2% hematocrit was used for each of the assays and incubated for 96 h before SYBR Green could be added to determine the fluorescence and ultimately the IC_{50} for MDL73811. Figure 3.1 illustrates the sigmodial graph of the IC_{50} determination for *Pf*3D7 treated with MDL73811.

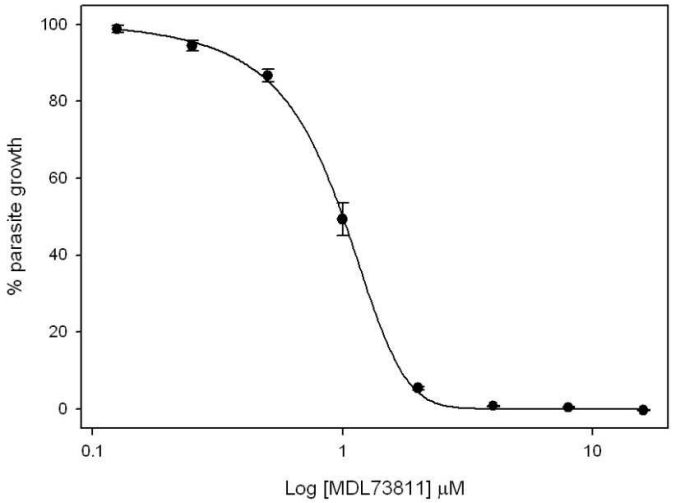

Figure 3.1: A concentration response curve for the IC_{50} determination of MDL73811.
Error bars are representative of the SEM, n = 4. R^2=0.99, IC_{50} = 0.96 µM ± 0.16 µM

An IC_{50} of 0.96 µM ± 0.16 µM were obtained for MDL73811 against the CQ sensitive *Pf*3D7 strain. Successful establishment of the IC_{50} of MDL73811 prompted the evaluation of the morphological impact of MDL73811 on the parasites. *Pf*3D7 parasites were treated with a concentration of 10 µM MDL73811 (~10×IC_{50}). This high concentration of MDL73811 against *Pf*AdoMetDC is used to ensure that parasites do not escape drug pressure, and were used for all experimental procedures to follow (Van Brummelen, 2009).

3.3.2 Morphological evaluation of *P. falciparum* 3D7 inhibited by MDL73811 over a complete life cycle

The entire Plasmodial life cycle was monitored morphologically over a 48 h period. *Pf*3D7 were treated just before invasion of erythrocytes. The media was changed every 12 h to minimise the negative influence of lactic acid on parasite growth. Morphological examination of the parasites

microscopically occurred at 2-3 hourly intervals (Figure 3.2 A and B). The complete morphological assessment of control parasites (untreated, UT) and 10 µM MDL73811-treated (T) parasites over a complete lifecycle of 48 h was followed (Figure 3.2). Both UT and T parasites remained morphologically similar from invasion (0 hours post-invasion, HPI) through the ring stage (0-18 HPI) and the early trophozoite stage (18-25 HPI) (Figure 3.2 A). This is further iterated by Figure 3.2 B which shows that the representative graphs of both UT and T parasites were identical during the ring and early trophozoite stages. Morphological arrest of MDL73811-treated parasites occurred between 25 and 30 HPI (Figure 3.2 A). According to the IDC transcriptome, the *Pf(adometdc/odc)* transcript is produced from 12 to 36 HPI with maximum expression at 24 HPI (Bozdech *et al.*, 2003). It is also within this period of maximum transcript expression of *Pf(adometdc/odc)* that the morphological arrest occurs. At 30 HPI the UT parasites differentiated into schizonts, while the T parasites clearly remained in the trophozoite stage without any further differentiation and remained in the trophozoite stage indefinitely (Figure 3.2 B). It is also visible that after 32 HPI the MDL73811-treated parasites became picnotic and remains picnotic over the rest of the life cycle and does not re-invade new erythrocytes (Figure 3.2 A). The MDL73811-treated parasites did not progress to a new life cycle and consequently did not form new ring stage parasites unlike the UT parasites that started a new life cycle after 48 h by releasing merozoites that invaded new erythrocytes that will ultimately form new ring stage parasites. This morphological assessment of the MDL73811-treated parasites furthered the notion that MDL73811 acts as a cytostatic drug even at concentrations of 10 µM MDL73811 (Van Brummelen, 2009).

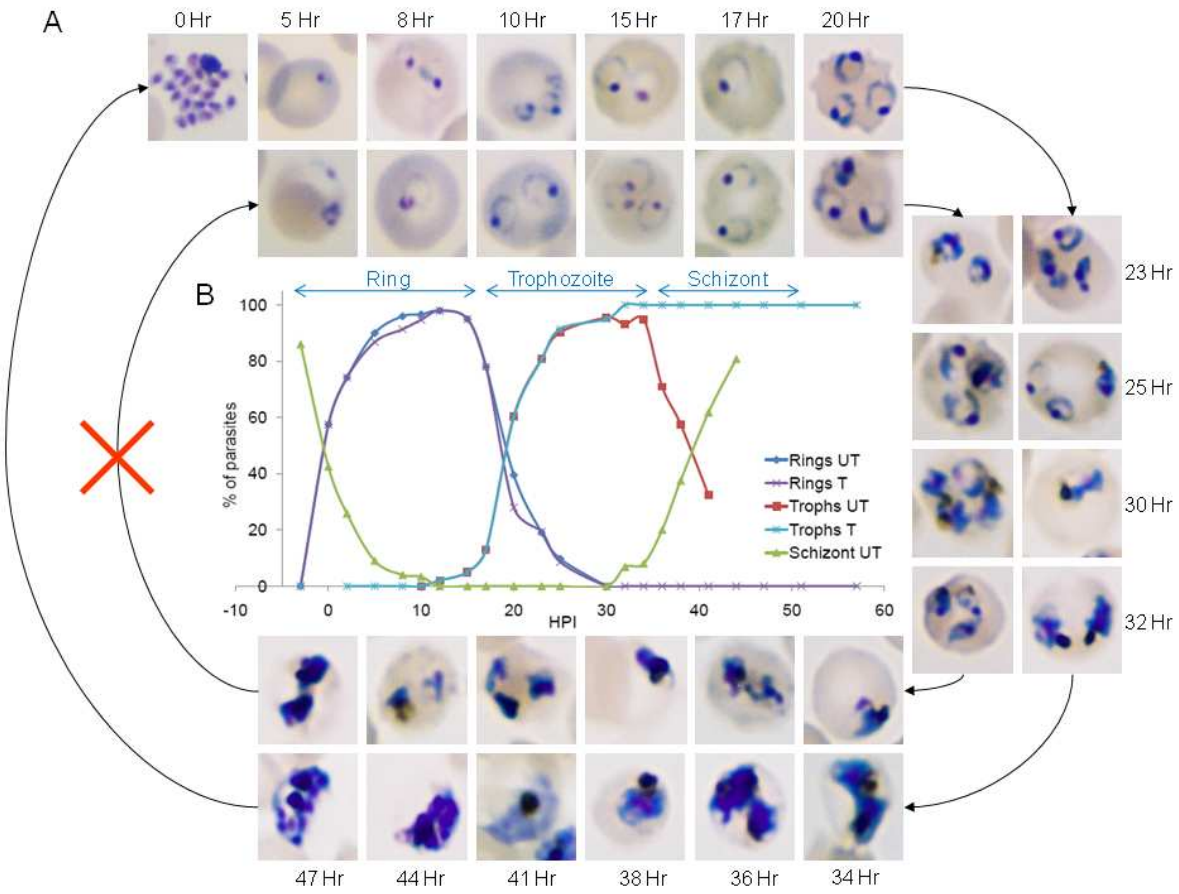

Figure 3.2: Morphology study of *Pf*3D7 parasites over a 48 hour life cycle.

(A)The outside of the circle illustrates the untreated parasites that will progress through schizogeny to develop into merozoites at approximately 46-52 hours and will ultimately invade new erythrocytes. The inside circle demonstrates the MDL73811-treated parasites, which will not develop into new merozoites, since these treated parasites are arrested during schizongeny from about 25 hours onwards. (B) A graphical illustration of the morphological arrest of MDL73811-treated and untreated *Pf*3D7 parasites. The light blue line is the trophozoite stage of the MDL73811-treated parasites that persist as trophozoites and does not develop into schizonts.

3.3.3 SDS-PAGE analysis of perturbed parasites and functional analysis of differentially regulated bands from 1-DE SDS-PAGE gels

Due to the fact that the transcript for *Pf*AdoMetDC/ODC is produced from 12 to 36 HPI with maximum transcript expression at 24 HPI (Bozdech *et al.*, 2003) and the morphological assessment that showed that morphological arrest of the MDL73811-treated parasites occurs between 25-30 HPI (Figure 3.2 A and B). Two time points (16 HPI (t_1) and 20 HPI (t_2)) were chosen that were before morphological arrest of the MDL73811-treated parasites and relating to the time at which the transcript for *Pf(adometdc/odc)* should already be expressed by the parasites and therefore the MDL73811 could take effect on *Pf*AdoMetDC. The perception was also that because these 2 time points were before a visible morphological arrest the 2 time points would be representative of drug

specific parasite response rather than life cycle differences. Therefore, the UT and T parasites were harvested at 16 HPI and 20 HPI for the proteomic study. The protein-containing supernatant and the insoluble protein pellet of both time points were run on SDS-PAGE gels to determine if differential protein expression did occur. Figure 3.3 is a representation of the 4 SDS-PAGE gels that each is representative of 1 biological replicate that were loaded in quadruplet. For both time points, 60 µg of the soluble protein-containing supernatant was loaded onto the SDS-PAGE gels. Due to the insoluble nature of the protein pellet the protein concentration could not be reliably determined and therefore 60 µl of each protein pellet were loaded onto the SDS-PAGE gels. All 4 gels were stained with Colloidal Coomassie Blue.

The SDS-PAGE gels were analysed using Quantity One 4.4.1 to detect possible differentially affected bands between the treated and untreated samples. Differentially affected bands were detected in both the soluble and insoluble fractions for the 2 time points, of which 17 bands were selected, and prepared for MS analysis (Figure 3.3, labelled numerically from 1-17). Since SDS-PAGE separation is limited to only molecular weight, it is extremely likely that one band may consist of various proteins of similar molecular weights. This is one of the essential reasons for separating the extracted peptides from each band of the SDS-PAGE gels with a reverse phase column before being identified by electrospray ionisation tandem mass spectrometry (ESI-MS/MS). The peptides and partial sequences were searched by Protein Pilot™ to identify the proteins present within each of the bands. The identified bands and their corresponding proteins are given in Table 3.3.

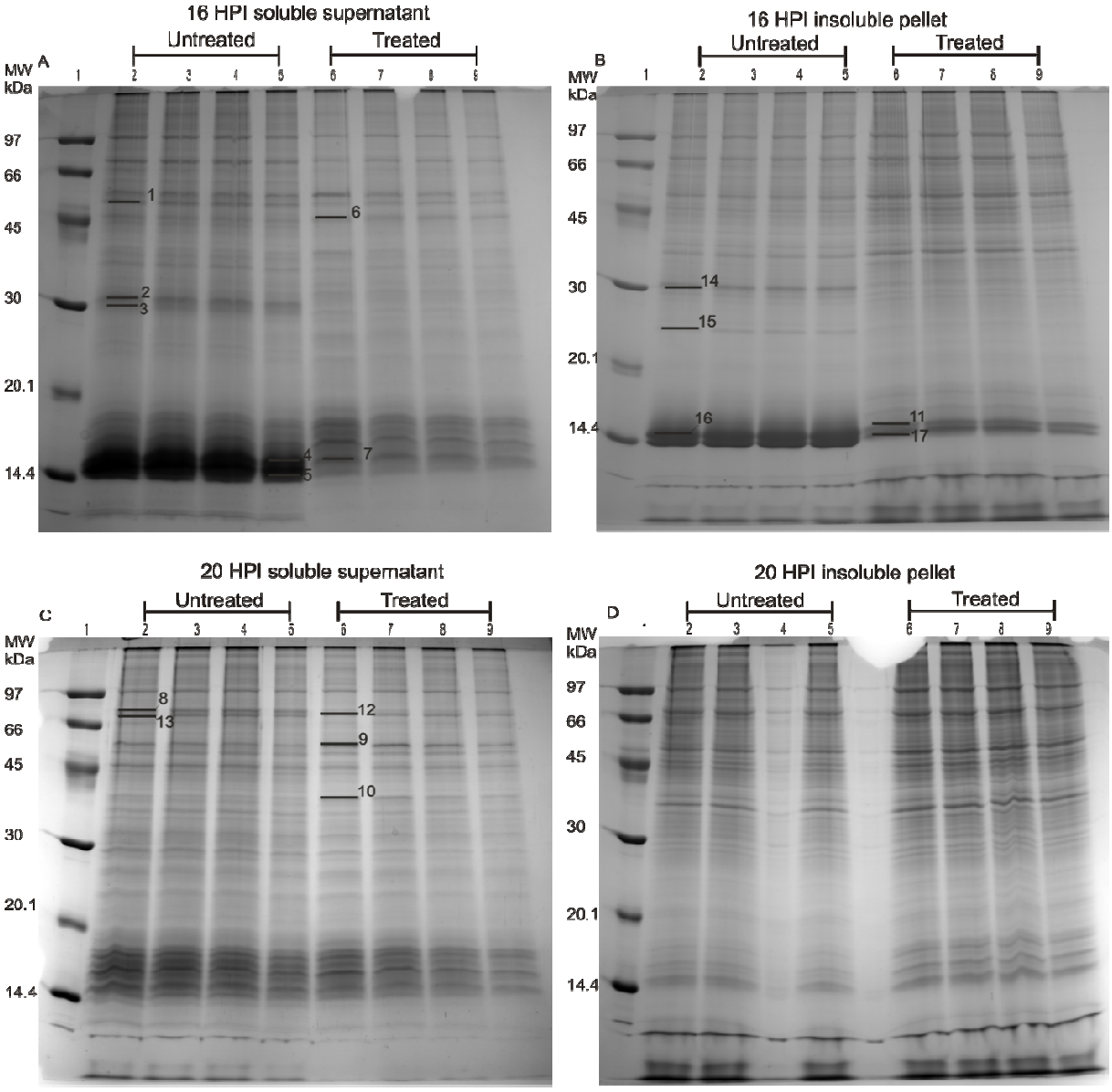

Figure 3.3: 1-DE SDS-PAGE gels for the soluble and insoluble protein fractions from the 2 time points investigated.

(A) 16HPI soluble supernatant, (B) 16 HPI insoluble pellet, (C) 20 HPI soluble supernatant, (D) 20 HPI insoluble pellet. Lanes are marked with numbers 1-9 on top of each gel. Lane 1 is always the molecular weight marker. Lanes 2-5 are the untreated samples and lanes 6-9 are the treated samples. Differentially affected bands that were used for MS analysis is marked on the gels with numbers 1-17.

Table 3.3: Differentially affected bands from AdoMetDC inhibited parasites identified from SDS-PAGE by LC-ESI-MS/MS

Band nr[a]	FC[b]	Accession nr[c]	PlasmoDB ID[d]	Name	MW	pI	Score[e]	%Cov[f]
				(A) Up-regulated bands				
6	1.4	Q8I431	PFE0350c	60S ribosomal subunit protein L4/L1, putative	46212	11.2	11.39	13.87
		Q8I4X0	PFL2215w	Actin I	41821	5.27	9.46	15.69
		Q8IJC6	PF10_0272	Ribosomal protein L3, putative	44222	10.89	5.64	9.59
9	2	Q8IJD0	PF10_0268	Merozoite capping protein 1	43936	10.45	11.68	15.27
		Q9TY94	PFB0445c	Helicase, putative pf	52224	5.84	11.68	2.41
10	3.5	Q8IDR9	PF13_0228	40S ribosomal subunit protein S6, putative	35385	11.19	4.63	8.50
				(B) Down-regulated bands				
1	-1.8	Q27727	PF10_0155	Enolase	48678	6.54	14.75	23.09
		Q8I0P6	PF13_0305	Elongation factor 1-alpha	48959	9.6	13.39	18.96
		Q8IL88	PF14_0359	Hypothetical protein	48470	7.2	1.69	
2	-18	P00915	—	Carbonic anhydrase 1 *(Homo sapiens)*	28870	6.59	14.96	36.78
		Q8IDQ9	MAL13P1.214	Phosphoethanolamine N-methyltransferase, putative	31043	5.28	3.5	5.26
		Q8IM10	PF14_0083	Ribosomal protein S8e, putative	25051	10.65	3.41	13.76
		Q8IIU8	PF11_0065	Ribosomal protein S4, putative	32355	10.55	2.33	3.55
		Q8I3T9	PFE0845c	60S ribosomal subunit protein L8, putative	28000	11.18	2.13	5.00
3	-6	P68871	—	Hemoglobin subunit beta *(Homo sapiens)*	15998	6.74	9.1	32.65
		P00915	—	Carbonic anhydrase 1 *(Homo sapiens)*	28870	6.59	5.71	13.03
4	-5	P68871	—	Hemoglobin subunit beta *(Homo sapiens)*	15998	6.74	0.02	84.83
		P02042	—	Hemoglobin delta chain *(Homo sapiens)*	16055	7.84	7.39	58.22
		Q7JSX6	PF11_0061	Histone H4, putative	11456	11.8	4.34	22.33
		Q8IIV1	PF11_0062	Histone H2B	13125	10.96	3.24	12.82
5	-3.4		—	Hemoglobin alpha chain *(Homo sapiens)*			0	82.14
		Q7JSX6	PF11_0061	Histone H4, putative	11456	11.8	6.16	33.01
		Q8ILN8	PF14_0205	Ribosomal protein S25, putative	15741	10.42	3.05	15.56
		Q8IIV1	PF11_0062	Histone H2B	13125	10.96	0	12.82
7	-5	P68871	—	Hemoglobin subunit beta *(Homo sapiens)*	15998	6.74	14.74	43.54
		Q7JSX6	PF11_0061	Histone H4, putative	11456	11.8	8.66	33.98
		Q8IIV1	PF11_0062	Histone H2B	13125	10.96	0	12.82
8	-1.3	P16452	—	Erythrocyte membrane band 4.2 protein *(Homo sapiens)*	77009	8.39	0	16.78
		Q8IB24	PF08_0054	Heat shock 70 kDa protein	73916	5.33	0	0.00
12	-1.3	Q8IB24	PF08_0054	Heat shock 70 kDa protein	73916	5.33	25.75	21.86

		Q8I2X4	PFI0875w	Heat shock protein	72388	4.93	7.73	6.13
13	-3.1	Q8IB24	PF08_0054	Heat shock 70 kDa protein	73916	5.33	20.58	13.44
		Q8I2X4	PFI0875w	Heat shock protein	72388	4.93	6.25	6.13
14	-3.9	P00915	—	Carbonic anhydrase 1 *(Homo sapiens)*	28870	6.59	19.7	44.44
		Q8IDQ9	MAL13P1.214	Phosphoethanolamine N-methyltransferase, putative	31043	5.28	6.76	18.05
		P00921	—	Carbonic anhydrase II *(Bos taurus)*	29114	6.41	3.58	10.77
		P00918	—	Carbonic anhydrase 2 *(Homo sapiens)*	29246	6.87	2.73	7.34
15	-3.4	P32119	—	Peroxiredoxin-2 *(Homo sapiens)*	21892	5.66	4.57	4.57
16	-4.4	P68871	—	Hemoglobin subunit beta *(Homo sapiens)*	15998	6.74	0.04	93.20
11	-4.4	P68871	—	Hemoglobin subunit beta *(Homo sapiens)*	15998	6.74	0	57.93
		Q7JSX6	PF11_0061	Histone H4, putative	11456	11.8	5.68	22.33
		Q8I467	PFE0165w	Actin depolymerizing factor, putative	13741	7.94	2.06	10.66
17	-0.9		—	CS185522 NID *(Homo sapiens)*			48.19	53.16
		Q7JSX6	PF11_0061	Histone H4, putative	11456	11.8	8.09	33.98
		Q8I5C5	PFL1420w	Macrophage migration inhibitory factor homolog, putative	12845	6.43	4.69	21.55

Proteins identified are sorted numerically according to the band number. [a]Band number corresponds to marked bands in Figure 3.5. [b]FC is the fold change for regulation of each differentially regulated band as determined by Quantity One 4.1.1 and is the intensity ratio for T/UT. All values given are significant ($p<0.05$).[c]Accession number is obtained from the SwissProt UniProt database. [d]PlasmoDB ID is obtained from the PlasmoDB 6.0 database. [e]Score is based on MS/MS searches done by the Protein Pilot™ software for LC-MS/MS. A score of more than 2.0 is considered significant ($p<0.05$). [f]Sequence coverage is given by Protein Pilot for detected peptide sequences.

Of the 17 bands that were cut for LC-ESI-MS/MS analysis, a total of 45 proteins were identified within these bands. This correlates to 29 unique proteins, of which 20 are unique Plasmodial proteins. Eleven of the unique Plasmodial proteins had a pI above 9.6 and would therefore normally not be detected on 2-DE due to the pI constraints associated with 2-DE. Of these 11 proteins, 7 proteins were ribosomal proteins that ranged in pI from 10-11.2, while the other 4 proteins included elongation factors and histone proteins that ranged in pI from 9.6 to 11.8 (Table 3.3). From the original 17 bands that were cut for MS-identification, 3 bands had an increased abundance and correlated to 6 proteins identified, while 13 bands had decreased abundance which correlated to 36 proteins identified. One band used for MS-identification showed no change in differential abundance between the treated and untreated samples and consisted of 3 identified proteins. It should be noted that although the bands are differentially regulated this is not necessarily true for all of the proteins that are identified for that particular band. This is because a band consists of more than 1 protein of which only 1 may be differentially regulated in abundance and the other proteins may be unchanged in abundance.

3.3.4 2-DE analysis of AdoMetDC inhibited parasites

The results obtained from SDS-PAGE analysis of both soluble and insoluble proteins fractions from AdoMetDC inhibited parasites confirmed the feasibility of the presence of differentially regulated proteins. This prompted the 2-DE analyses of the soluble proteins over 2 time points to enable a more comprehensive proteomic view of the overall protein regulation induced by the inhibition of AdoMetDC. For first dimensional IEF separation, each of the sixteen 18 cm IPG strips was loaded with 400 µg total protein each and run overnight before being placed on large format gels for second dimensional separation to achieve maximal spot separation. The gels were then stained with Flamingo Pink, scanned using the Versadoc 3000 scanner and finally analysed using PD Quest 7.1.1 to determine statistically significant differences between UT and T samples.

PD Quest program is able to distinguish between a protein-related spot and background dust speckles and automatically removes speckles from the dataset. This was also manually determined for all spots reported on each of the gels where speckles have very distinguishable sharp peaks, and protein-related spots have nice gaussian shapes and are therefore easily distinguished (Figure 3.4).

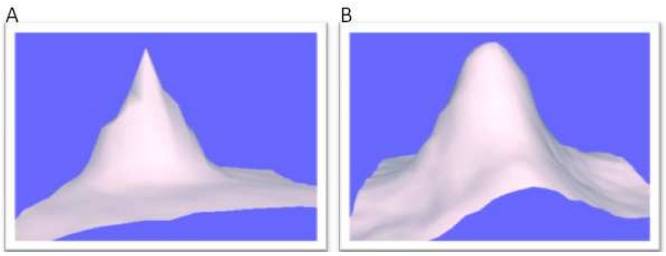

Figure 3.4: The difference between a real protein spot and a dust speckle.
A: speckle, B real protein spot.

Spots were detected by automated detection and matching by the software. All the spots detected and matched were manually verified to limit the possibility of false positive spot matching. A master image was created from the 8 gels (4 × UTt_1 and 4 × Tt_1 gels) present within the first time point (t_1) (Figure 3.5). Similarly a master image containing all the spot information for all 8 gels for the second time point (t_2) was also created (not shown).

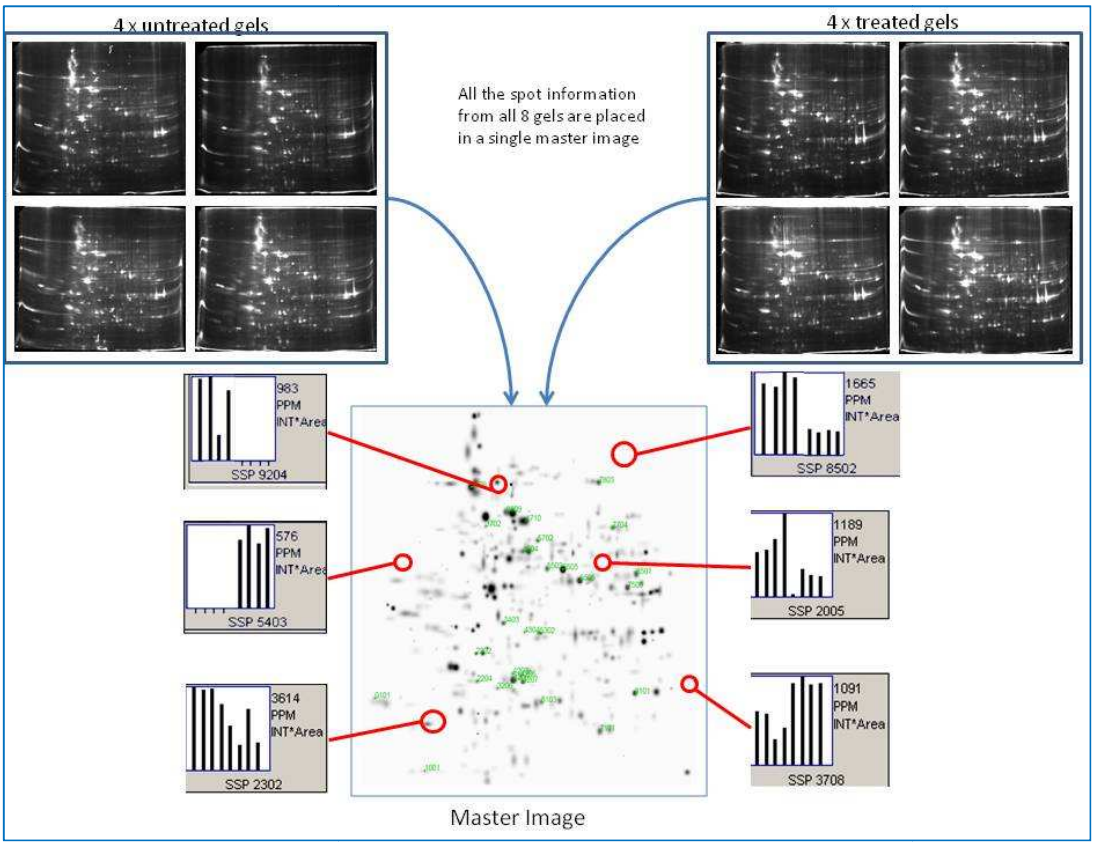

Figure 3.5: Creation of the master image used for detection of differentially affected proteins.
The spot information of the 4 UT gels and the 4 T gels are combined into a single master image that contains all the spot information on all 8 gels it consists of. The user can then select any spot on the master image and a graph will appear that will give information of the exact same spot in all of the 8 different gels that the master image consists of. Therefore for SSP9204 the master image contains information that the spot is only present in each of the 4 UT gels and completely absent in all of the 4 T gels. Each bar represents the normalised intensity for the specific spot from each of the 8 gels.

The master image contains all the spot information for both the untreated as well as the treated gels. The master image is used to obtain all the information needed for differentially affected protein spots. Basically, the master image is used to answer questions asked by the user on differential regulation of spots (Figure 3.6).

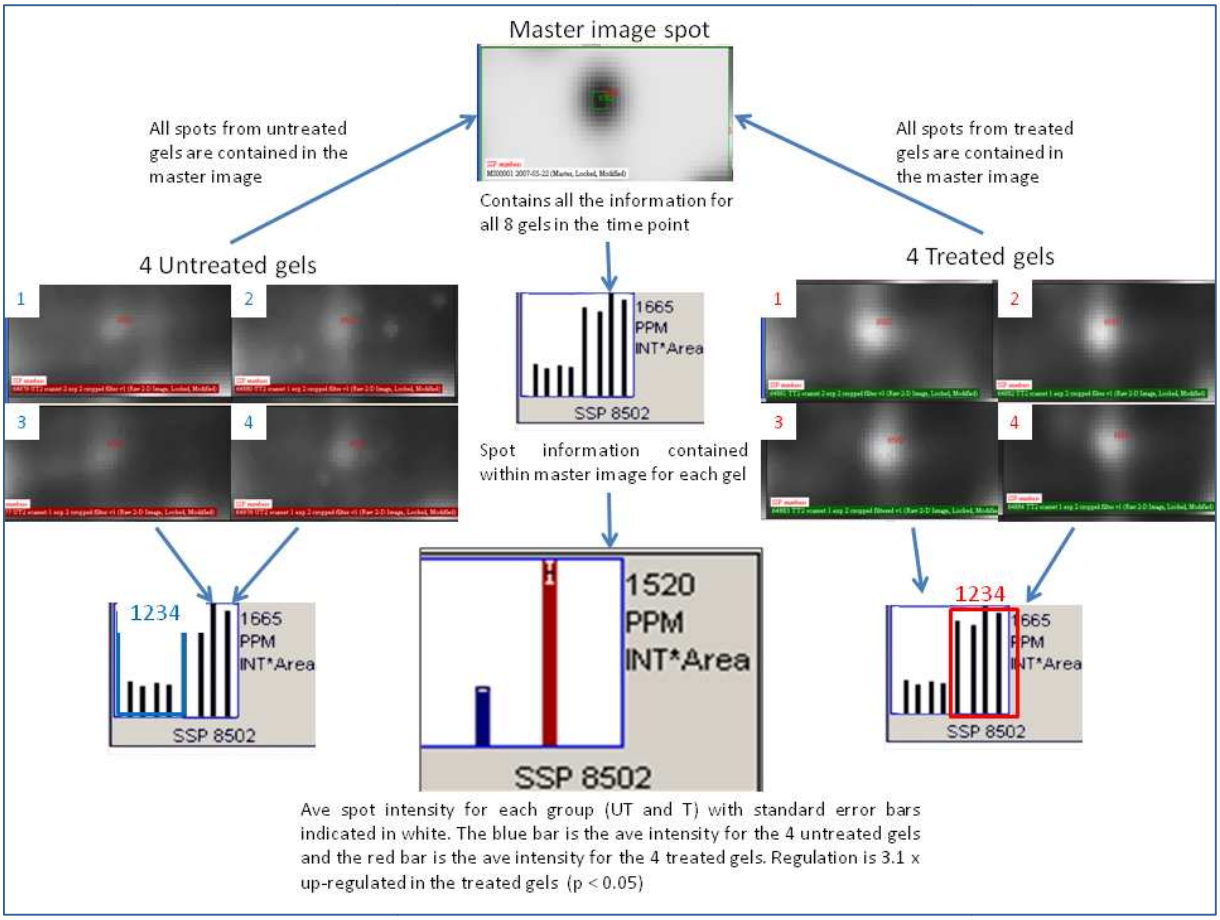

Figure 3.6: Determination of differentially affected protein spots between the treated and untreated groups using the master image.

The master image contains a single spot with the information from the single spot from each of the 4 T and 4 UT gels (numbered 1-4 in blue for UT and 1-4 in red as T). The master image then is able to give the information in graphical form for a specific spots, in which each of the 8 gels is represented as a different bar on the graph (marked 1-4 in blue on the bar graphs for UT samples and correlate to gel number, and similarly for the T samples marked in red on the bar graphs and gel images. Finally, for differential protein abundance determination the 4 values of the UT samples are taken as an average (blue bar), which is similarly done for the treated sample (red bar). A standard error is also calculated and given as a white error bar on each of the graphs. This is then used to determine differential protein abundance ($p < 0.05$).

The master image is created from all 8 gels. Therefore, if a spot in present within all 8 gels (4 × UTt_1 and 4 × Tt_1 gels) then the master image contains only a single spot in similar position on its image, but that spot contains the information for all 8 spots from the 8 gels. This information contained for each spot can be extracted from the master image and converted to graph format. The bars on the graph represent each of the 8 gels with the first 4 bars representative of the UT sample

and the last 4 bars representative of the T samples (Figure 3.6). To determine differentially affected protein spots ($p < 0.05$), the average value is taken and together with a standard error-of-the-mean to determine significance of protein spots between the 2 groups.

A summary of the data for both time points are given in Table 3.4. A good gel match rate (number of spots that are matched for each individual gel) of 96-98% was achieved for t_1 and t_2. The master match rate was 88% for t_1 and 58% for t_2. The master match rate is defined as the matching number of spots of each individual gel to the number of spots contained within the master image. The high match rate obtained for t_1 indicates that the differences observed between the T and UT samples are relatively small. The lower master match rate for t_2 is indicative of progression of the UT samples when compared to the T samples due to AdoMetDC inhibition. When even later time points were to be investigated the discrepancies between the UT and the T sample would increase due to life cycle stage differences, hence resulting in an even lower match rate. The correlation coefficient for t_1 between the T and UT groups was 0.719 while for t_2 it decreased to 0.664.

Table 3.4: Data obtained from PD Quest 7.1.1 after spot detection of both the UT and T gels for t_1 and t_2.

Condition	t_1	t_2
Master image spot count	369	450
UT vs T group corr coeff	0.719	0.664
Ave match rate per gel	98% ± 0.7[a]	96% ± 1.8[a]
Ave master match rate	88% ± 4.4[a]	58% ± 6.0[a]
Ave spots per gel	325	272

[a]Match rates are given as an average of all eight gels per time point with the standard deviation.

For statistical purposes, replicate groups were created in which the 4 gels of the UT samples are grouped together as the UT group and similarly for the 4 gels from the T samples. The information contained within the master image is then used to ask questions to the master image. This is usually done to determine spots that are differentially affected ($p<0.05$) between the 2 groups. Both graphical and numerical data can be obtained for each regulated spot and are given in a report. Figure 3.7 depicts a graphical representation of spot quantification where this protein spot was increased 3.1-fold in the T group compared to the UT group. Each of the bars given on the graph contains the information for all 4 gels of that specific group (UT blue bar vs T red bar), and are statistically significant.

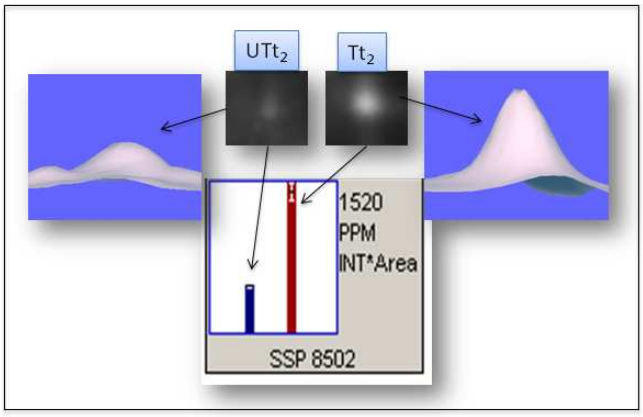

Figure 3.7: Differential protein spot abundance determined by PD Quest.

SSP 8502 is the number given to the spot by the software. This spot is increased 3.1-fold in protein abundance in Tt_2 as compared to UTt_2. The spots as seen on the 2-DE gels are on top of the figure with the white spot on the black background. To the sides of each of the two spots are a 3-D representation of the spots and the graphs for the spots are given at the bottom of the figure. The blue bar represents the UTt_2 group that contains all the information for the 4 gels within this group. The red bar is representative of the 4 gels within the Tt_2 group.

In a similar fashion as described above, the total number of differentially affected protein spots for both time points was determined and is given in Table 3.5. A total of 55 spots were identified as differentially regulated in Tt_1 ($p<0.05$). This indicates that 17% (55/325) of the proteome of AdoMetDC inhibited parasites are differentially affected within the first time point (late rings). For the second time point, 64 (52 + 7 + 5) spots fulfilled the criteria of $p<0.05$ according to the student t-test. Therefore, Tt_2 resulted in 24% (64/272) of the AdoMetDC inhibited proteome to be affected. Therefore in total, 119 protein spots were identified as differentially affected in the AdoMetDC inhibited proteome.

Table 3.5: The total number of differentially affected protein spots for the 2 time points

Regulation type	t_1	t_2
Present only in T[a]	0	7
Absent only in T[a]	0	5
Differentially regulated spots[b]	55	52
Total nr of differentially regulated spots	**55**	**64**

[a]These are spots that are only present in either the T or UT group. [b]Spots that are at differentially regulated and considered as significant ($p<0.05$) according to the student t-test.

3.3.5 Protein identification of differentially affected protein spots from the AdoMetDC inhibited proteome

The differentially affected protein spots identified by the software were subsequently cut from the gels and prepared for MALDI-Q-TOF MS/MS analysis. For identification of each of the protein spots, a PMF was first obtained from the protein, which was immediately followed by MS/MS analysis of the 50 highest peaks from the PMF for that particular protein. An example of a PMF and

the MS/MS data obtained for AdoMet synthase is given in Figure 3.8. A series of peptides were obtained that ranged from 600 – 3400 Da. From this range of peptides, the peptide with a m/z value of 1401.8 was used to illustrate the effect of MS/MS in which the amino acid sequence could now be obtained. The collision gas is used in the collision chamber of the MALDI-Q-TOF to fragment the peptide into its different amino acids. From Figure 3.8 B it can be seen that the y_1-ion is arginine (R) since it has a m/z value of 175.1, and was expected since trypsin cleaves at either lysine or arginine residues. Each amino acid has a specific mass and therefore by analysing the MS/MS spectra (Figure 3.8 B), the amino acid sequence can be obtained from the spectra, which in this case is a peptide that consists of 15 amino acids that are marked y_1 to y_{15} or b_1 to b_{15} (Figure 3.8 C). Protein scores of more than 45 was considered as significant for identification of the protein ($p<0.05$).

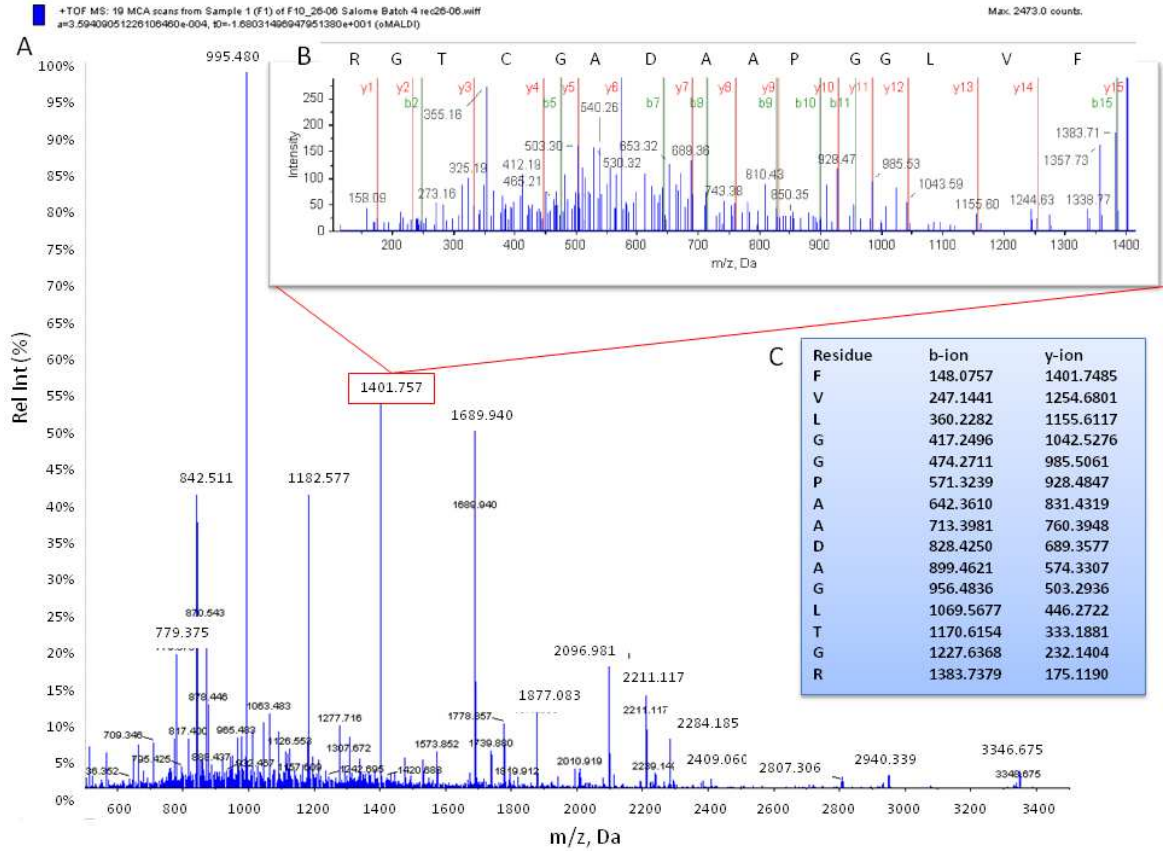

Figure 3.8: The MS spectra of S-adenosylmethionine synthase.

The bottom of the figure is a representation of a PMF that was obtained. The insert depicts the amino acid sequence (FVLGGPAADAGCTGR) of a single PMF peak (1401.757) as determined by MS/MS with the values of both the b- and y-ions and the masses of each. A protein score of 863 were obtained in the MS-ion search mode of MASCOT. Sequence coverage of 40% was obtained for this protein and the amino acid sequences of 14 peptides were used for scoring.

In a similar way as described above, the differentially affected protein spots identified by PD Quest for Tt_1 and Tt_2 were cut and trypsinised before being subjected to MALDI-Q-TOF MS/MS and finally the MS-spectra submitted to MASCOT for protein identification. Differentially affected protein spots that were positively identified by MS/MS analyses are depicted in Figure 3.9 for both Tt_1 and Tt_2. The differential fold-change of each identified protein spot as well as the MW, pI, MS/MS scores is given in Table 3.6. To minimise the possibility of false positive identifications, a protein was only considered to have a positive identification if the protein score was more than 45 ($p<0.05$), together with at least 10% sequence coverage, with at least 5 peptides for each particular protein.

Of the 119 differentially regulated spots that were identified for Tt_1 and Tt_2 (Table 3.6), a total of 91 protein spots were identified of which 53 protein spots were from Tt_1 and 38 protein spots were from Tt_2. For the first time point (Tt_1) 25 protein spots were identified by MS/MS to have increased protein abundance together with 28 protein spots that had decreased protein abundance. This accounts for a total of 15 Plasmodial protein spots with increased protein abundance of which 14 were unique Plasmodial protein groups. Amongst the 28 decreased abundance protein spots, 23 were unique Plasmodial proteins. A total of 20 protein spots had increased protein abundance (15 unique Plasmodial proteins) and 12 protein spots (6 unique Plasmodial proteins) had decreased protein abundance in Tt_2, together with 6 protein spots that were either absent or present in only one of the samples (either UTt_2 or Tt_2). Therefore, the 91 protein spots identified by MS/MS consisted of 75 Plasmodial protein spots (82% Plasmodial protein spots) and finally accounted for a total of 46 unique Plasmodial protein groups over the 2 time points (Table 3.6).

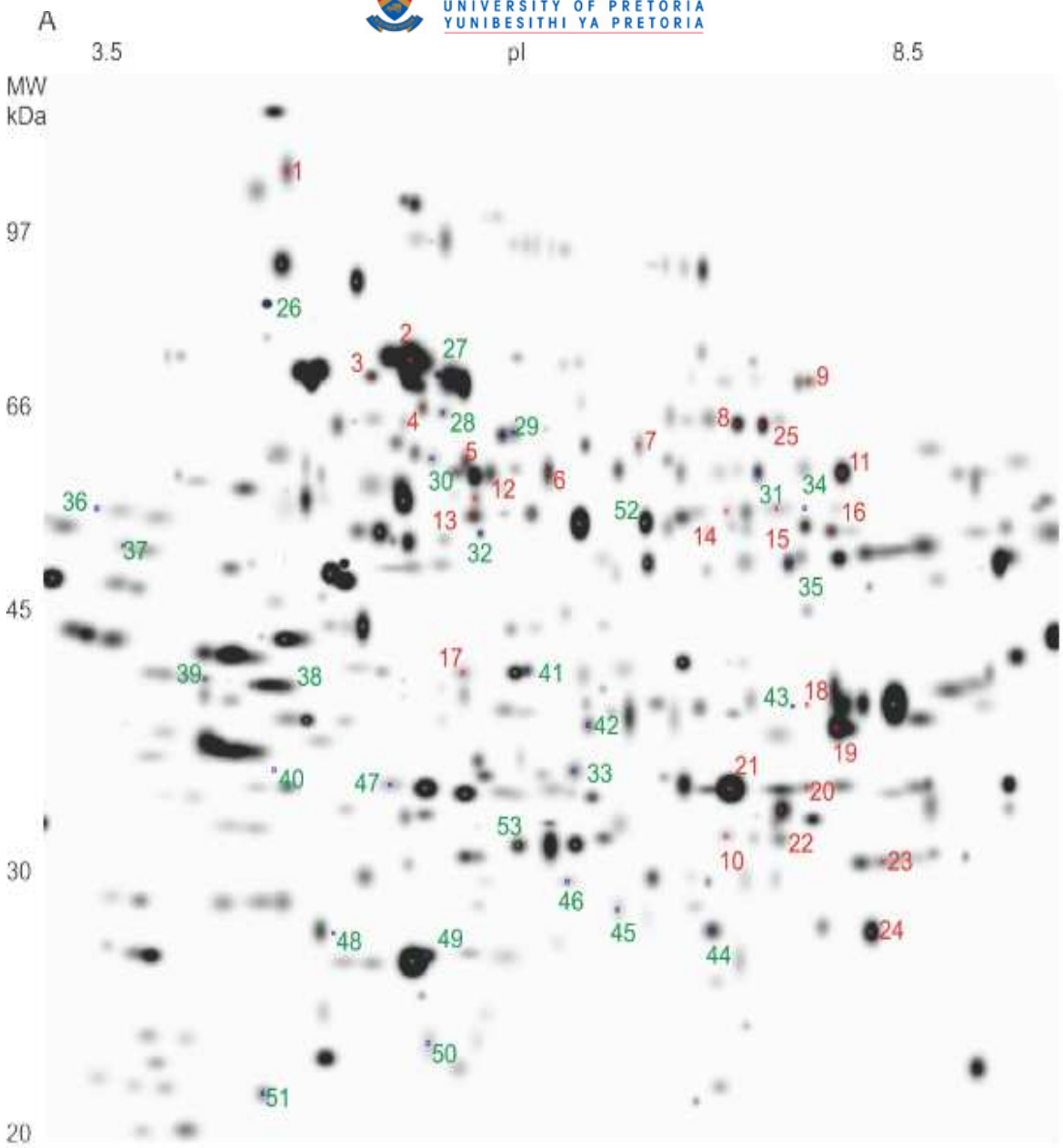

Figure 3.9 A: Master images of the Tt_1 (16 HPI) with the differentially affected protein spots that were identified indicated.

Numbers given in red is indicative of increased protein abundance of the protein spots while green is decreased protein abundance of protein spots. The numbers correspond to the numbers given in Table 3.6.

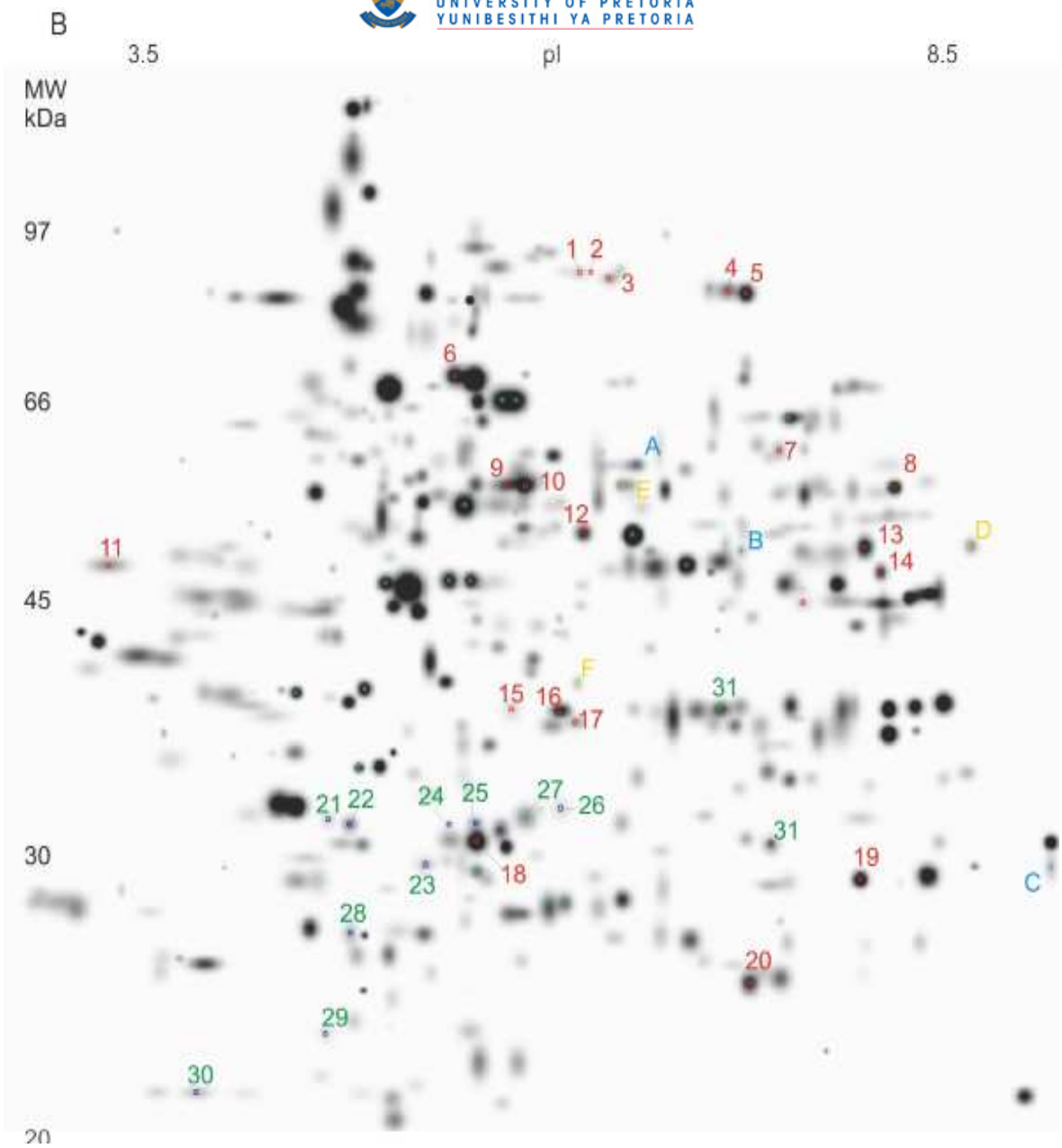

Figure 3.9 B: Master images of the Tt_2 (20 HPI) with the differentially affected protein spots that were identified indicated.

Numbers given in red is indicative of increased protein abundance of the protein spots while green is decreased protein abundance of protein spots. Protein spots that were only detected in one of either the T or UT sample were only found in Tt_2 and are marked A-F, with blue indicative of spots that are present in Tt_2 and yellow indicative of spots that were absent in Tt_2. The numbers correspond to the numbers given in Table 3.6.

Table 3.6: Protein spots identified by MS/MS for the AdoMetDC inhibited proteome at Tt_1 and Tt_2.

Spot nr[a]	FC[b]	Accession nr[c]	Plasmo DB[d]	Name	Mr	pI	Mascot score MS/MS[e]	Seq cover[f]	Match[g]
(A) Protein spots with increased protein abundance Tt_1									
20	18.0	P00915	—	Carbonic anhydrase 1 *(Homo sapiens)*	28778	6.63	531	50	8
21	1.7	P00915	—	Carbonic anhydrase 1 *(Homo sapiens)*	28620	6.65	845	58	11
22	1.5	P00918	—	Carbonic anhydrase 2 *(Homo sapiens)*	28802	6.63	320	30	7
14	3.3	P04040	—	Catalase *(Homo sapiens)*	59816	6.95	425	22	9
25	1.6	P04040	—	Catalase *(Homo sapiens)*	59816	6.95	659	29	15
8	2.2	Q8I6S6	MAL8P1.17	Disulfide isomerase, putative	55808	5.56	693	35	15
5	2.2	Q9TY94	PFB0445c	eIF4A-like helicase, putative	52647	5.68	251	13	6
13	2.0	Q27727	PF10_0155	Enolase	48989	6.21	313	18	7
15	5.1	O96940	PF14_0164	Glutamate dehydrogenase ($NADP^+$) (1)	53140	7.48	283	17	8
16	2.1	O96940	PF14_0164	Glutamate dehydrogenase ($NADP^+$) (2)	53140	7.48	497	30	13
18	2.2	Q8T6B1	PF14_0598	Glyceraldehyde-3-phosphate dehydrogenase	37068	7.59	131	11	3
23	2.1	P38545	PF11_0183	GTP-binding nuclear protein ran/tc4	24974	7.72	485	55	12
2	2.7	Q8IB24	PF08_0054	Heat shock 70 kDa protein	74382	5.51	1378	34	23
3	3.5	P19120	—	Heat shock 70 kDa protein *(Bos taurus)*	71454	5.37	579	20	11
10	1.3	P68871	—	Hemoglobin subunit beta *(Homo sapiens)*	16112	6.71	870	37	19
6	1.4	Q8IL11	PF14_0439	Leucine aminopeptidase, putative.	68343	8.78	172	14	7
19	1.5	Q71T02	PF13_0141	L-lactate dehydrogenase	34314	7.12	611	43	12
7	1.3	Q8IDC7	MAL13P1.283	MAL13P1.283 protein	58506	6.09	261	10	6
9	10	Q8I3Y8	PFE0585c	Myo-inositol 1-phosphate synthase, putative	69639	7.11	454	25	14
11	1.3	Q8IJ37	PFI1300w	Putative pyruvate kinase	56480	7.5	732	37	16
12	2.8	Q13228	—	Selenium binding protein 1 *(Homo sapiens)*	52928	5.93	140	12	6
24	1.8	P02769	—	Serum albumin *(Bos taurus)*	71274	5.82	510	16	10
1	2.0	P00915	—	Spectrin alpha chain, erythrocyte *(Homo sapiens)*	282024	4.98	889	24	9
17	1.6	Q8I3X4	PFE0660c	Purine nucleoside phosphorylase, putative	27525	6.07	412	47	9
4	2.0	Q03498	MAL13P1.271	V-type ATPase, putative	69160	5.51	291	19	10
(B) Protein spots with decreased protein abundance Tt_1									
45	-1.8	Q8IJT1	PF10_0111	20S proteasome beta subunit, putative	30862	5.18	150	9	4
44	-1.4	Q9N699	PF14_0368	2-Cys peroxiredoxin	21964	6.65	540	59	8
41	-2.3	Q8IJD4	PF10_0264	40S ribosomal protein, putative	30008	5.91	152	11	3
33	-1.4	P07738	—	Bisphosphoglycerate mutase *(Homo sapiens)*	30027	6.1	461	43	10
30	-3.5	Q9TY94	PFB0445c	eIF4A-like helicase	52647	5.68	589	26	10
32	-4.1	Q27727	PF10_0155	Enolase	48989	6.21	373	18	7

51	-10.0	Q8I603	PFL0210c	Eukaryotic initiation factor 5a, putative	17791	5.42	159	27	4
40	-7.0	Q8I6U4	PF11_0165	Falcipain 2	56405	7.12	212	12	6
34	-2.2	O96940	PF14_0164	Glutamate dehydrogenase (NADP+)	53140	7.48	212	15	6
46	-1.6	Q8MU52	PF14_0187	Glutathione s-transferase	24888	5.97	47	11	2
43	-2.8	O96369	PF14_0598	Glyceraldehyde-3-phosphate dehydrogenase	37068	7.59	302	25	7
38	-2.0	Q8IM15	PF14_0078	HAP protein	51889	8.05	645	34	13
26	-3.5	Q8IC05	PF07_0029	Heat shock protein 86	86468	4.94	1153	25	24
29	-2.7	Q8IJN9	PF10_0153	Hsp60	62911	6.71	870	37	19
36	-4.7	Q8I608	PFL0185c	Nucleosome assembly protein 1, putative	42199	4.19	293	16	7
49	-2.9	P32119	—	Peroxiredoxin-2 *(Homo sapiens)*	21918	5.67	515	41	10
47	-1.5	Q8IDQ9	MAL13P1.214	Phosphoethanolamine N-methyltransferase, putative	31309	5.43	252	22	5
35	-1.5	P27362	PFI1105w	Phosphoglycerate kinase	45569	7.63	214	15	5
39	-2.2	Q8I6V3	PF14_0077	Plasmepsin 2	51847	5.36	72	6	3
42	-1.4	Q9U570	MAL8P1.142	Proteasome beta-subunit	31080	6.00	212	22	7
31	-1.3		PFF1300w	Putative pyruvate kinase	56480	7.5	633	28	15
48	-3.3	Q8I2Q0	PFI1270w	Putative uncharacterized protein PFI1270w	24911	5.49	327	26	6
52	-1.3		PFI1090w	S-adenosylmethionine synthetase	45272	6.28	863	40	14
27	-3.4		—	Serum albumin *(Bos taurus)*	71274	5.82	620	24	15
37	-4.2	Q4KKW9	—	Solute carrier family 4, anion exchanger, member 1 *(Homo sapiens)*	101978	5.13	189	7	4
50	-1.7	P00441	—	Superoxide dismutase *(Homo sapiens)*	16154	5.7	219	37	4
53	-1.8	Q8I3X4	PFE0660c	Purine nucleoside phosphorylase, putative	27525	6.07	572	36	10
28	-3.2	Q03498	MAL13P1.271	V-type ATPase, putative	69160	5.51	184	13	7
				(C) Protein spots with increased protein abundance Tt_2					
20	1.9	Q9N699	PF14_0368	2-Cys peroxiredoxin	21964	6.65	504	72	11
15	3.6	Q8IJD4	PF10_0264	40S ribosomal protein, putative (1)	29856	6.15	27	11	3
16	1.6	Q8IJD4	PF10_0264	40S ribosomal protein, putative (2)	30008	5.91	267	24	8
9	5.9	Q97TY94	PFB0445c	eIF4A-like helicase, putative (1)	52647	5.68	320	23	8
10	2.1	Q97TY94	PFB0445c	eIF 4A-like helicase, putative (2)	52646	5.68	62	42	14
4	4.7	Q8IKW5	PF14_0486	Elongation factor 2 (1)	94545	6.36	96	4	4
5	2.0	Q8IKW5	PF14_0486	Elongation factor 2 (2)	94546	6.78	657	26	18
12	1.4	Q8IJN7	PF10_0155	Enolase	48989	6.21	408	20	7
17	11.1	Q95W62	PFD0615c	Eryhrocyte membrane protein 1 (fragment)	13608	6.96	51	38	7
7	8.9	Q8ILA4	PF14_0341	Glucose-6-phosphate isomerase	67610	6.78	61	28	14
13	2.0	O96940	PF14_0164	Glutamate dehydrogenase (NADP+)	53140	7.48	336	28	11
6	2.2	Q8IB24	PF08_0054	Heat shock 70 kDa protein	74382	5.33	861	33	18
11	8.0	Q8IAW8	MAL8P1.95	Hypothetical protein MAL8P1.95	37933	4.13	385	25	8

14	3.1	Q71T02	PF13_0141	Lactate dehydrogenase	34000	8.5	100	12	3
1	8.1	Q8IEK1	MAL13P1.56	M1 family aminopeptidase (1)	126552	7.3	102	26	23
2	2.4	Q8IEK1	MAL13P1.56	M1 family aminopeptidase (2)	126552	6.68	124	25	25
3	4.6	Q8IEK1	MAL13P1.56	M1 family aminopeptidase (3)	126552	7.3	107	23	23
18	1.7	Q8IDQ9	MAL13P1.214	Phosphoethanolamine N-methyltransferase, putative	31309	5.28	722	48	13
19	1.3	Q8IIG6	PF11_0208	Phosphoglycerate mutase, putative	28866	8.3	401	36	10
8	2.3	Q8IJ37	PFF1300w	Putative pyruvate kinase	56480	7.5	101	51	16
				(D) Protein spots with decreased protein abundance Tt_2					
28	-1.6	O97249	PFC0295c	40S ribosomal protein S12, putative (1)	15558	4.9	85	14	2
30	-1.9	O97249	PFC0295c	40S ribosomal protein S12, putative (2)	15558	4.9	217	36	5
26	-2.1	Q8IM55	PF14_0036	Acid phosphatase, putative	35824	5.98	63	5	2
27	-1.4	Q8I4X0	PFL2215w	Actin-1 (1)	42272	5.27	359	22	7
32	-2.0	Q8I4X0	PFL2215w	Actin-1 (2)	42272	5.17	81	42	12
31	-2.4	P00915	—	Carbonic anhydrase 1 *(Homo sapiens)*	28620	6.65	70	20	4
21	-24.0	Q8I6U4	PF11_0165	Falcipain 2, putative (1)	56481	7.9	47	23	10
22	-2.3	Q8I6U4	PF11_0165	Falcipain-2, putative (2)	55804	7.49	56	24	11
23	-3.3	Q8ILV5	PF14_0138	Hypothetical protein	23889	5.49	53	9	2
24	-3.8	Q8IDQ9	MAL13P1.214	Phosphoethanolamine N-methyltransferase, putative (1)	31043	5.43	69	9	2
25	-1.8	Q8IDQ9	MAL13P1.214	Phosphoethanolamine N-methyltransferase, putative (2)	31043	5.28	177	22	5
29	-2.6	Q8I5T3	PFL0590c	P-type ATPase, putative	135214	6.13	54	18	16
				(E) Protein spots that were either present or absent in Tt_2					
A	On	Q8IDJ8	PF13_0262	Lysine tRNA ligase (EC 6.1.1.6)	68003	7.02	100		17
B	On	S51042		tat binding protein homolog malaria parasite	49859	6.86	52		12
C	On	Q8IDC6	MAL13P1.284	Pyrroline-5-carboxylate reductase (EC 1.5.1.2)	28816	8.13	61		9
D	Off	AAN36874	PF14_0261	Proliferation associated protein 2g4 putative	43327	7.54	63		12
E	Off	Q6LF74	PFF1155w	Hexokinase (EC 2.7.1.1)	56081	6.72	44		10
F	Off	Q8IKW5	PF14_0486	Elongation factor 2	94545	6.36	74		17

Proteins identified are sorted alphabetically according to name with isoforms grouped together and the number of isoforms per protein is marked in brackets next to the protein name. [a]Spot number corresponds to marked spots on the master image of ring stage parasites. [b]FC is the fold change for protein abundance of each spot either increased (+ value) or decreased (- value) compared to the untreated sample as determined by PD Quest 7.1.1. All values given are significant ($p<0.05$). [c]Accession number is obtained from the SwissProt UniProt database. [d]PlasmoDB ID is obtained from the PlasmoDB 6.0 database. [e]Mascot scores are based on MS/MS ion searches and is only taken when the score is significant ($p<0.05$). [f]Sequence coverage is given by Mascot for detected peptide sequences. [g]Matched is the number of peptides matched to the particular protein.

3.3.6 1-DE SDS-PAGE and 2-DE gels as complementary proteomic techniques to obtain maximal proteome information

A total 46 unique Plasmodial protein groups were identified with 2-DE as differentially affected in addition to the 20 unique Plasmodial protein groups identified using a 1-DE approach (Section 3.3.3). Of these 66 unique Plasmodial protein groups, only 5 unique Plasmodial protein groups were shared between the 2 approaches followed (Figure 3.10). These include heat shock protein 70 kDa (PF08_0154), enolase (PF10_0155), PEMT (MAL13P1.214), eIF4A-like helicase protein (PFB0445c) and actin-1 (PFL2215w). The 15 Plasmodial proteins that were identified with only 1-DE would not normally be detected on 2-DE due to the pI and molecular weight constraints associated with the use of 2-DE. Similarly, 41 Plasmodial protein groups were only detected on the 2-DE gels, which proves its superior separation ability. The use of both 1-DE and 2-DE therefore complemented the proteins that could be identified.

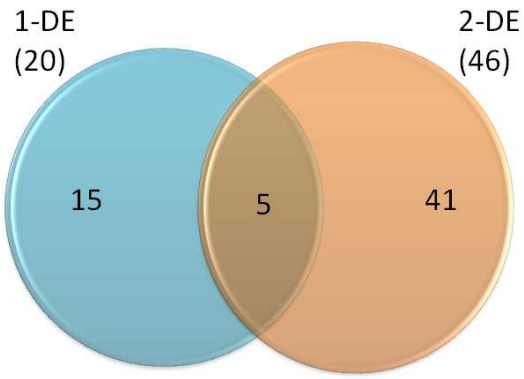

Figure 3.10: Correlation between Plasmodial proteins identified from 2 complimentary proteomic approaches.

3.3.7 Hierarchical clustering of differentially expressed proteins from the proteome of AdoMetDC inhibited parasites.

Hierarchical clustering of the differentially affected proteins identified by MS was performed for both time points (Figure 3.11). Only 2 clusters were obtained for the AdoMetDC inhibited proteome dataset because the T sample was always compared to the UT sample in order to determine differential regulation of the spots or proteins, therefore a differentially regulated spot has either increased or decreased abundance. Interestingly, the polyamine-related proteins and oxidative stress proteins tended to cluster together (Figure 3.11, marked in red and blue).

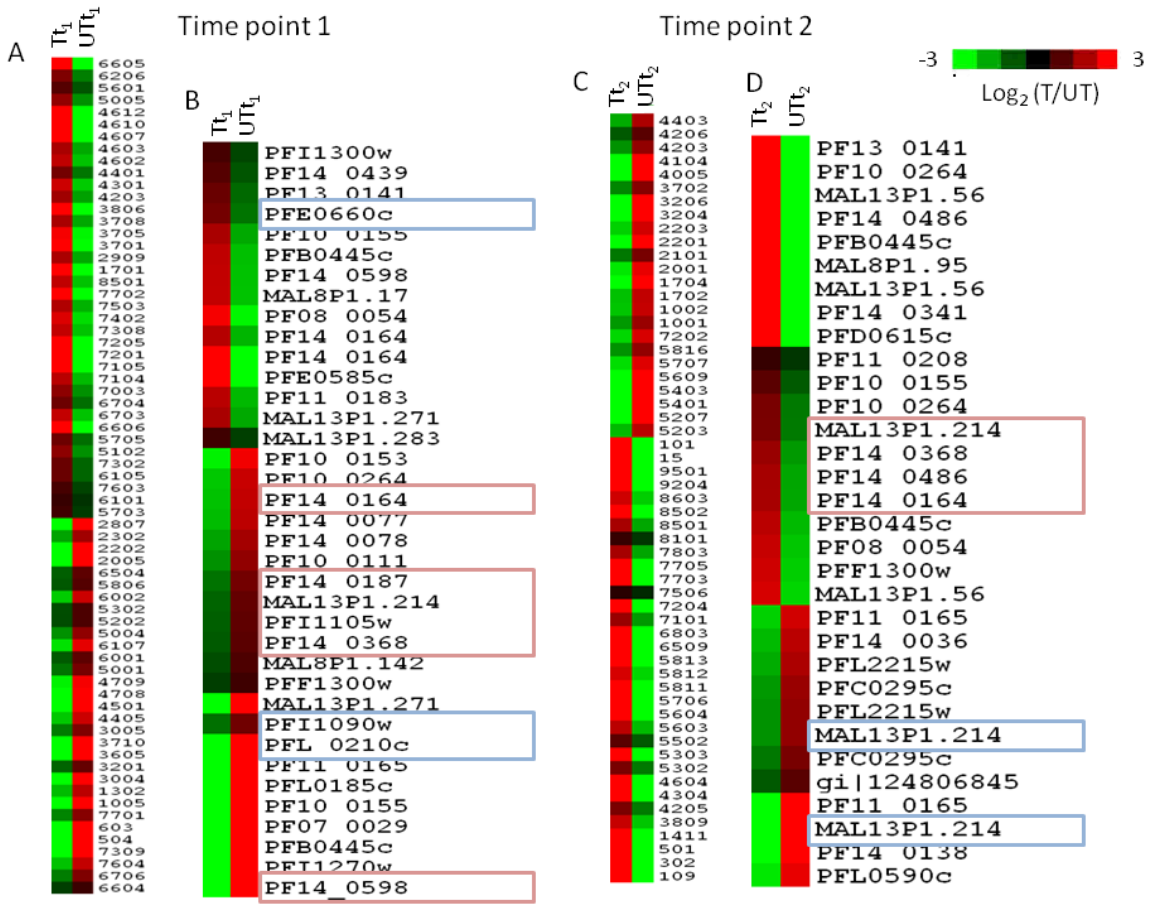

Figure 3.11: Hierarchical clustering of the differentially affected spots and identified proteins from AdoMetDC inhibition for two time points.

(A)All the differentially affected spots from t_1. (B) Clustering of the identified proteins from t_1. (C) All the differentially affected spots from t_2. (D) Clustering of the identified proteins from t_2. The pink blocks are representative of mostly oxidative stress proteins and the blue blocks are representative of mostly polyamine-related proteins. Unregulated spots were not included into the hierarchical clustering of any of the time points.

3.3.8 Functional classification of the differentially affected proteins identified from the proteome of AdoMetDC inhibited parasites.

The 46 unique Plasmodial protein groups were sorted according to their GO annotations that were obtained from PlasmoDB 6.0, and then grouped into their respective GO functions (Table 3.7, Figure 3.12). Each protein was only grouped into a single category despite the fact that some proteins may be representative of more than one GO annotation. The functional GO groupings were validated with MADIBA (www.bi.up.ac.za/MADIBA/).

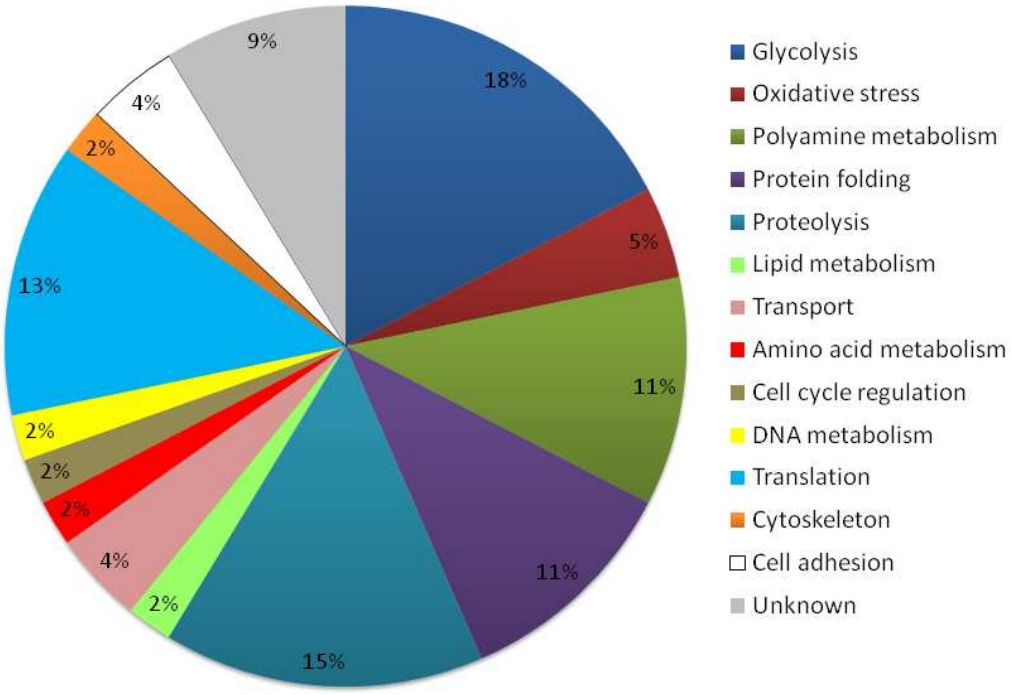

Figure 3.12: GO annotation for the regulated spots of both time points.
GO annotations were obtained from PlasmoDB 6.0 and classified according to biological process in MADIBA.

Only 9% (4/46 proteins) of the AdoMetDC inhibited proteome dataset that was identified by MS was regarded as hypothetical proteins with unknown functions. This is probably due to the small portion of unique Plasmodial protein groups that were identified (46 proteins). Of the 46 unique Plasmodial protein groups identified by MS, 18% were associated with glucose metabolism. Some of the other groups that were highly represented included protein folding (11%), polyamine metabolism (11%), proteolysis (15%), translation (13%) and oxidative stress (5%). Polyamine and methionine metabolism included 5 differentially expressed proteins. Of these 5 unique Plasmodial proteins groups that were differentially affected, 3 proteins had increased protein expression and included PNP (PFE0660c, 1.6-fold), pyrroline-5-carboxylate reductase (MAL13P1.284, present in Tt_2) and 1 isoform of PEMT (MAL13P1.214, 1.7-fold). Two other isoforms of PEMT both had decreased transcription (-1.5-fold and -3.8-fold respectively). The protein expression of AdoMet synthetase (PFI1090w, -2.3-fold), eukaryotic initiation factor 5a (eIF5A, PFL0210c, -10-fold) and another protein isoform of PNP (PFE0660c, -1.8-fold) had decreased abundance in the first time point (Figure 3.9 and Table 3.7). Unfortunately, in the second time point, AdoMet synthase and OAT which is in close proximity of each other on the 2-DE gel overlapped and were saturated possibly due to the increased protein abundance of OAT and could therefore not be quantitated.

Some of the other proteins that were differentially affected included eIF4A-like helicase protein (PFB0445c) that was detected as 2 isoforms at Tt_1 (2.2-fold and -3.5-fold) and 1 isoform at Tt_2 (5.9-fold) and seemed to be gradually increased in abundance over time. Several heat shock proteins were detected at both time points that included heat shock protein 70 kDa (PF08_0054, 2.7-fold Tt_1 and 2.2-fold Tt_2) that were increased in abundance at both time points, heat shock protein 86 (PF07_0029, -3.5-fold) and heat shock protein 60 (PF10_0153, -2.7-fold) that were both decreased in abundance at Tt_1 (Table 3.7).

Table 3.7: Biological functions of the differentially regulated proteins identified from the 2-DE gels from the AdoMetDC inhibited proteome.

PlasmoID[a]	Product name	Time point[b]	FC[c]	Min exp time HPI[d]	Max exp time HPI[d]
	Glycolysis				
PF10_0155	Enolase (1)	t_1	2	38	16
PF10_0155	Enolase (2)	t_1	-4.1	38	16
PF14_0598	Glyceraldehyde-3-phosphate dehydrogenase (1)	t_1	2.2	42	27
PF14_0598	Glyceraldehyde-3-phosphate dehydrogenase (2)	t_1	-2.8	42	27
PF13_0141	Lactate dehydrogenase	t_1	1.5	42	26
PFI1105w	Phosphoglycerate kinase	t_1	-1.5	38	19
PFF1300w	Putative pyruvate kinase	t_1	-1.3	41	26
PF10_0155	Enolase	t_2	1.4	38	16
PF14_0341	Glucose-6-phosphate isomerase	t_2	8.9	37	16
PF13_0141	Lactate dehydrogenase	t_2	3.1	42	26
PF11_0208	Phosphoglycerate mutase, putative	t_2	1.3	38	11
PFF1300w	Putative pyruvate kinase	t_2	2.3	41	26
	Polyamine metabolism				
PFE0660c	Purine nucleoside phosphorylase, putative (1)	t_1	1.6	4	22
PFE0660c	Purine nucleoside phosphorylase, putative (1)	t_1	-1.8	4	22
PFI1090w	S-adenosylmethionine synthetase	t_1	-1.3	12	32
MAL13P1.214	Phosphoethanolamine N-methyltransferase, putative	t_1	-1.5	10	33
PFL0210c	Eukaryotic initiation factor 5a, putative	t_1	-10	42	26
MAL13P1.214	Phosphoethanolamine N-methyltransferase, putative (1)	t_2	-3.8	10	33
MAL13P1.214	Phosphoethanolamine N-methyltransferase, putative (2)	t_2	1.7	10	33
MAL13P1.284	Pyrroline-5-carboxylate reductase	t_2	10		
	Protein folding				
MAL13P1.283	MAL13P1.283 protein	t_1	1.3	36	18
MAL8P1.17	Disulfide isomerase, putative	t_1	2.2	43	32
PF10_0153	Hsp60	t_1	-2.7	1	21
PF07_0029	Heat shock protein 86	t_1	-3.5	46	22
PF08_0054	Heat shock 70 kDa protein	t_1	2.7	42	23
PF08_0054	Heat shock 70 kDa protein	t_2	2.2	42	23
	Proteolysis				
PF10_0111	20S proteasome beta subunit, putative	t_1	-1.8		
PF11_0165	Falcipain 2	t_1	-7	36	19
PF14_0078	HAP protein	t_1	-2	38	19
PF14_0439	Leucine aminopeptidase, putative.	t_1	1.4	1	19
PF14_0077	Plasmepsin 2	t_1	-2.2	38	18
MAL8P1.142	Proteasome beta-subunit	t_1	-1.4	1	31
PF11_0165	Falcipain 2	t_2	-24	36	19
MAL13P1.56	M1 family aminopeptidase (1)	t_2	8.1	33	17
MAL13P1.56	M1 family aminopeptidase (2)	t_2	4.6	33	17

MAL13P1.56	M1 family aminopeptidase (3)	t_2	2.4	33	17
	Lipid metabolism				
PFE0585c	Myo-inositol 1-phosphate synthase, putative	t_1	10	10	34
	Proton transport				
MAL13P1.271	V-type ATPase, putative (1)	t_1	2	35	24
MAL13P1.271	V-type ATPase, putative (2)	t_1	-3.2	35	24
	Amino acid metabolism				
PF14_0164	Glutamate dehydrogenase (NADP+) (1)	t_1	5.1	28	43
PF14_0164	Glutamate dehydrogenase (NADP+) (2)	t_1	-2.2	28	43
PF14_0164	Glutamate dehydrogenase (NADP+) (3)	t_2	2	28	43
	Cell cycle regulation				
PF11_0183	GTP-binding nuclear protein ran/tc4	t_1	2.1	42	30
	DNA metabolism				
PFB0445c	eIF4A-like helicase, putative (1)	t_1	2.2	41	16
PFB0445c	eIF4A-like helicase, putative (2)	t_1	-3.5	41	16
PFL0185c	Nucleosome assembly protein 1, putative	t_1	-4.7	23	46
PFB0445c	eIF4A-like helicase, putative	t_2	5.9	41	16
	Translation				
PF10_0264	40S ribosomal protein, putative	t_1	-2.3	41	11
PFC0295c	PFC0295c	t_2	-1.6	41	11
PF10_0264	40S ribosomal protein, putative	t_2	3.6	41	11
PF14_0486	Elongation factor 2	t_2	4.7	46	17
	Oxidative stress				
PF14_0368	2-Cys peroxiredoxin	t_1	-1.4	41	26
PF14_0187	Glutathione s-transferase	t_1	-1.6	37	21
PF14_0368	2-Cys peroxiredoxin	t_2	1.9	41	26
	Hypotheticals				
PFI1270w	Putative uncharacterized protein PFI1270w	t_1	-3.3		
PF14_0036	PF14_0036	t_2	-2.1	2	18
MAL8P1.95	Hypothetical protein MAL8P1.95	t_2	8	37	18
	Cytoskeleton				
PFL2215w	Actin I	t_2	-1.4	15	39
	Cell adhesion				
PF14_0138	Hypothetical protein	t_2	-3.3	11	31
PFD0615c	Eryhrocyte membrane protein 1 (fragment)	t_2	11.1	31	46
	Cation transport				
PFL0590c	P-type ATPase, putative	t_2	-2.6	28	41

Proteins are sorted according to their GO classifications. [a]PlasmoDB ID is obtained from the PlasmoDB 6.0 database. [b]Time point is the time point at which the specific protein is differentially expressed. [c]FC is the fold change for protein abundance of each spot either increased (+ value) or decreased (- value) compared to the untreated sample as determined by PD Quest 7.1.1. All values given are significant ($p<0.05$). [d]The maximum and minimum transcript expression times for each of the proteins as given in the PlasmoDB 6.0 database. Isoform identified in a time point is given in brackets.

3.3.9 Changes in protein abundance in the proteome of AdoMetDC inhibited parasites over time.

The protein abundance of some of the differentially regulated proteins in the AdoMetDC inhibited proteome was investigated over time (Tt_1 and Tt_2), to determine a possible trend in protein expression. Some of the proteins that are closely involved in methionine and polyamine biosynthesis were investigated over time and could be divided into 3 main groups (Figure 3.13).

Proteins that increased in abundance over time, included 2-Cys peroxiredoxin (PF14_0368), heat shock protein 60 kDa (PF10_0153), pyruvate kinase (PFF1300w) and pyrroline-5-carboxylate reductase (MAL13P1.284) (Figure 3.13 A). The other proteins decreased in abundance over time and were therefore grouped together which included heat shock protein 70 (PF08_0054), adenosine deaminase (PF10_0289) and PNP (PFE0660c) (Figure 3.13 B). Three protein isoforms were identified for PEMT (MAL13P1.214) of which 1 isoform increased in abundance, while the other 2 isoforms that were identified for PEMT (MAL13P1.214) decreased in abundance over time (Figure 3.13 C). Polyamine-related proteins that were not included in the groups were eIF5A (PFL0210c) and AdoMet synthase (PFI1090w) that both had decreased protein abundance at Tt_1, but could not be identified at Tt_2. Together, this regulation of protein abundance indicates that AdoMetDC inhibition does influence the parasite over time, with the majority of the detected polyamine-related proteins having decreased protein abundance over time. Comparisons between transcript and protein abundance and possible transcriptional regulatory mechanisms will be discussed in more detail in Chapter 5.

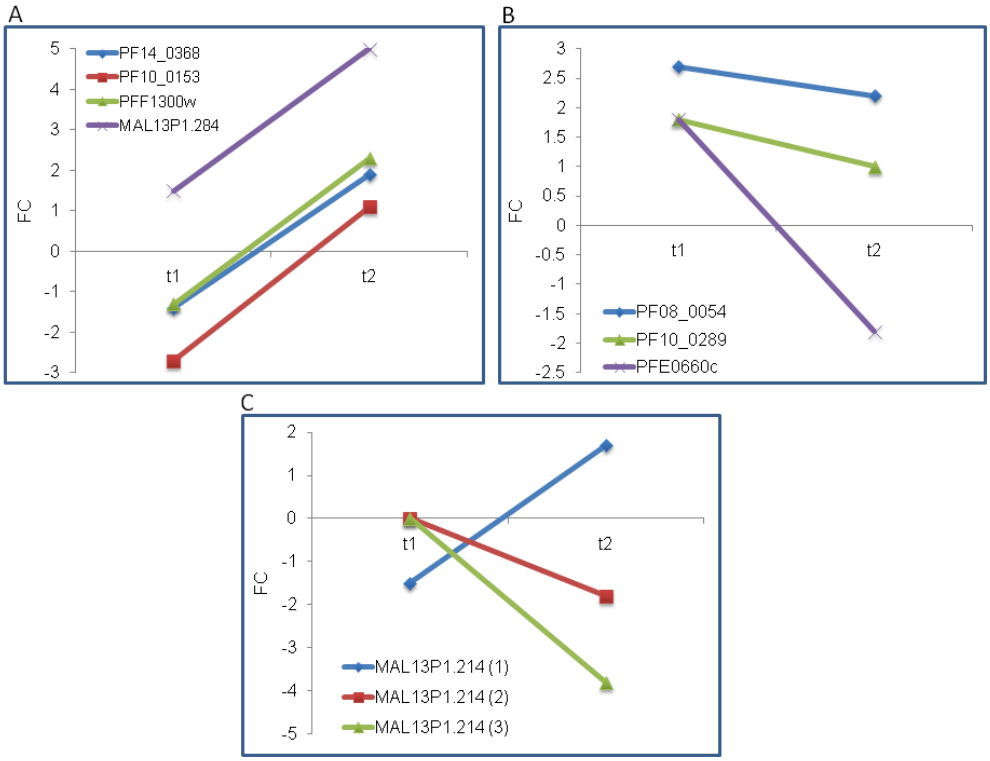

Figure 3.13: Differential regulation of proteins over time in the AdoMetDC inhibited proteome.

(A)Proteins that increased in abundance over time and include 2-Cys peroxiredoxin (PF14_0368), heat shock protein 60 kDa (PF10_0153), pyruvate kinase (PFF1300w), pyrroline-5-carboxylate reductase (MAL13P1.284). (B) Proteins that decreased in abundance over time and include heat shock protein 70 (PF08_0054), adenosine deaminase (PF10_0289), purine nucleoside phosphorylase (PFE0660c). (C) Three isoforms of phosphoethanolamine N-methyltransferase (MAL13P1.214) that changed in abundance over time.

3.3.10 Validation of differential proteomic data

To validate the 2-DE data, selective western blot analysis was performed on PEMT and M1-family aminopeptidase. Even though Flamingo Pink is a fluorescent stain that is semi-quantitative and has good linearity, it is of utmost importance to validate proteomic data with a sensitive and accurate method to confirm protein levels obtained from the 2-DE gels. The 2-DE gels and 2-DE western blot analysis showed clearly that PEMT consists of several isoforms that are grouped in close proximity of each other (Figure 3.14).

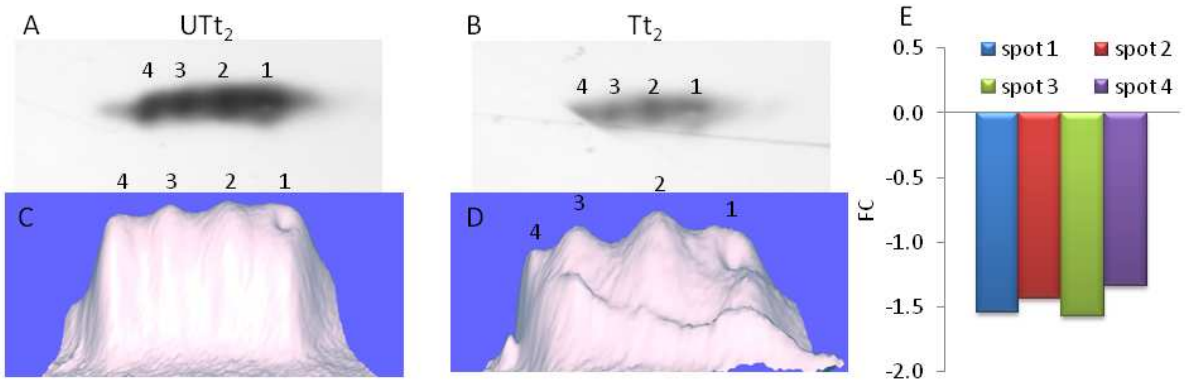

Figure 3.14: 2-DE Western blot of phosphoethanolamine N-methyltransferase.

The 3-D images were created by PD Quest. 2-DE was done on 13 cm IPG strips pH3-10 L, and run on a 16x18 cm gel. (A) The immunoblot for UTt_2, (B) immunoblot for Tt_2, (C) 3-D image of the spots in A, (D) 3-D image of the spots in B. The numbers on top of the spots is indicative of the number of isoforms detected. (E) The fold change calculated for each of the 4 different isoforms. All isoforms have decreased protein abundance. The intensity of each of the spots was determined using PD Quest. The fold change was then calculated for each individual spot to determine differential regulation of each of the 4 spots detected.

The 2-DE western blot of PEMT confirmed the decreased abundance of the protein in the treated sample as well as the existence of at least 4 isoforms that could be detected. All 4 isoforms decreased in protein abundance (spot 1: -1.6-fold, spot 2: -1.4-fold, spot 3: -1.6-fold, and spot 4: -1.3-fold) according to the 2-DE western blot. 2-DE analysis of PEMT revealed 3 protein isoforms of PEMT that was identified by MS/MS (Figure 3.9 and Table 3.6). Two isoforms decreased in protein abundance in Tt_2 (-3.8-fold and -1.7-fold) and 1 protein isoform had an increase in protein abundance (1.7-fold). The AdoMetDC inhibited 2-DE gels for Tt_2 were done on 18 cm IPG strips while the 2-DE western blot for validation was done on a 13 cm IPG strip. The 2-DE gels for the AdoMetDC inhibited proteome revealed a cluster of 6 spots in close proximity of which 3 were used for MS identification and subsequently identified as PEMT. The difference in separation power between the 2 strips could be the reason that 4 isoforms were detected on the 2-DE western blot since some of the protein isoforms and spots may overlap.

Three isoforms of M1-family aminopeptidase was detected in Tt_2 all with increased protein abundance according to the 2-DE analysis (Figure 3.9 and Figure 3.15). Therefore, the increased protein abundance that was determined for M1-family aminopeptidase in Tt_2 by 2-DE was also validated by 1-DE western blot analysis. Depicted in Figure 3.15 is the conventional 1-DE western blot that confirmed the increased protein expression determined on the 2-DE gels for the AdoMetDC inhibited proteome. Since only 1-DE western blot was done the data was analysed using Quantity One 4.4.1 by determination of the intensity of each band. The blot showed increased protein abundance for the Tt_2 sample compared to UTt_2, which was therefore sufficient for the validation of the proteomic results.

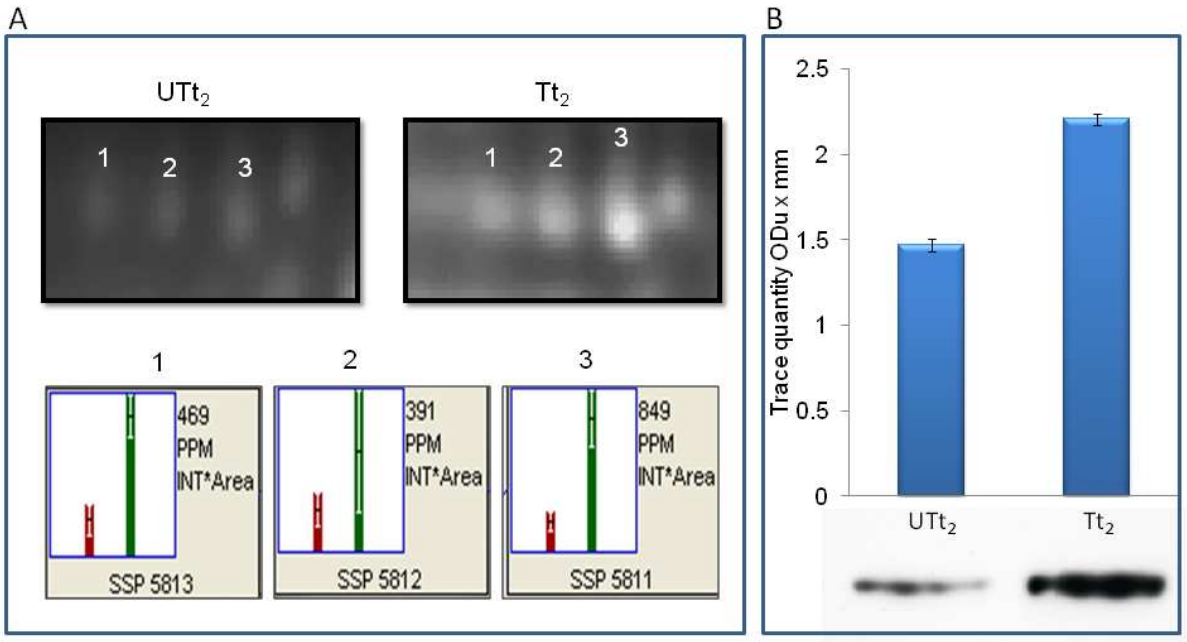

Figure 3.15: 1-DE western blot validation of the protein abundance of M1-family aminopeptidase that was detected on 2-DE at Tt_2.

A: The 3 M1-family aminopeptidase isoforms identified on the 2-DE gel with MS/MS. The 3 M1-family aminopeptidase isoforms are marked on the representative gels with the numbers 1-3. Spot number 1 has a fold change of 8.1, spot number 2 has a fold change of 2.4 and spot number 3 has a fold change of 4.6. At the bottom of the figure is the corresponding PD Quest data for each of the 3 isoforms. The PD Quest data indicates the red bar as the average intensity for the spot for UTt_2 and the green bar as the corresponding spot for Tt_2. The data are representative of 4 gels each for the T and UT gels, and the error bars are represented by the SEM. B: Graphical representation of the immunoblot data obtained. At the bottom of the graphs are the immunoblot showing UTt_2 and Tt_2. The data are for 2 immunoblots and the error bars are representative of SEM.

3.4 Discussion

An IC_{50} of 0.96 µM was determined for MDL73811 against a CQ sensitive strain of *P. falciparum* (*Pf*3D7) using the fluorescence based MSF assay. This is similar to previous results that made use of fluorescence activated cell sorting (FACS) in which an IC_{50} of 0.8 µM was determined (Van Brummelen, 2009). Another study, in which a [^{3}H]hypoxanthine assay was used, the IC_{50} of MDL73811 against *Pf*3D7 was determined to be 3µM (Das Gupta *et al.*, 2005), which is 3 times more than both the values obtained from different methodologies in our laboratory. The results obtained within this study supports the sensitivity of the SYBR green assay for DNA detection (Rengarajan *et al.*, 2002) especially in *Plasmodium*. A possible reason for the discrepancy between the IC_{50} obtained for MDL73811 during this study using the MSF-assay, and the IC_{50} of 3 µM obtained using the [^{3}H]hypoxanthine assay (Das Gupta *et al.*, 2005), may be the differences in incubation times for the assays. The [^{3}H]hypoxanthine assay is completed over a period of 48 h compared to the MSF-assay which spans over 96 h. The increased incubation time of the MSF-assay may therefore result in lower IC_{50}-values.

For all the experiments a dosage of 10 µM (~10×IC_{50}) MDL73811 was used as treatment. This high dosage was used due to the cytostatic nature of MDL73811 on the Plasmodial parasites, and to ultimately ensure complete arrest of all the parasites (Van Brummelen, 2009). The use of lower dosages of MDL73811 treatment in the ring stage, resulted in only incomplete arrest (Van Brummelen, 2009). This is due to the wide synchronisation window of 8-12 h. The MSF-assay used here to determine the IC_{50} of MDL73811, indicated complete arrest at the high concentration of 10 µM (~10×IC_{50}) MDL73811, and no parasite growth when performed over a 96 h period. The high concentration of MDL73811 (10 µM) is not toxic to the parasites, especially since in all the experiments performed within this study (Chapters 3, 4 and 5) the parasites were exposed to MDL73811 for only short periods of time, and therefore the MDL73811 only exert a cytostatic effect. The cytostatic nature of MDL73811 was also demonstrated previsiously with the use of propidium iodide stained parasites. Staining of MDL73811-treated parasites revealed no membrane permeability and therefore confirmed the cytostatic nature of MDL73811 (Van Brummelen, 2009) which can also be reversed by the addition of spermidine and spermine to MDL73811-treated parasites (Wright *et al.*, 1991).

After establishment of the IC_{50} of MDL73811 a morphology study commenced to determine the morphological point of parasite arrest. According to the IDC data the transcript of *Pf(adometdc/odc)* is already produced from about 12 HPI (morphologically in the ring stage) onwards with the maximum transcript production at 24 HPI (trophozoites) and transcript production levels decreasing

soon afterwards with the minimal transcript production at 53 HPI (schizont and merozoites stages). Observation of MDL73811-treated parasites revealed morphological arrest at about 25-30 HPI in the late trophozoite stage, when the drug inhibits the AdoMetDC domain of AdoMetDC/ODC. This was also demonstrated previously with the complete enzymatic inhibition of *Pf*AdoMetDC with 5 µM MDL73811 in which MDL73811-inhibited parasites revealed no decarboxylase activity in either the ring or late trophozoites stages but is also not toxic to the parasite (Van Brummelen, 2009).

Differential regulation of the proteome was observed in Tt_1 and Tt_2. This was especially illustrated by the fact that the correlation for UTt_1:Tt_1 was 0.719 compared to UTt_2:Tt_2 that was 0.664. Direct comparisons were made between the time points, although later time points would have prompted the use of the t_0 reference strategy (van Brummelen *et al.*, 2009) rather than the direct comparison employed here.

This proteomic study employed the use of both 1-DE and 2-DE gel-based methods to determine differentially regulated proteins. It was clearly illustrated that the use of both techniques were complementary to each other since only 5 unique Plasmodial protein groups were shared between the 1-DE AdoMetDC inhibited proteome data and the 2-DE AdoMetDC inhibited proteome data. This was somewhat unexpected since it would have been considered that more proteins would be shared between the 2 gel-based protein separation techniques employed. Although 1-DE does not have the powerful protein separation ability of 2-DE gels, the 1-DE approach does have the advantage that pI constraints do not impact on the proteins that are separated. This was illustrated in that the majority of the proteins that were detected in the 1-DE approach would never be detected on 2-DE due to the pI constraints associated with IPG strips. The pI of some of the identified proteins ranged from 9.6 to 11.8, and even with the use of extremely basic IPG strips it would have been difficult to detect such extremely basic proteins on 2-DE. Therefore, the use of complementary gel-based protein separation techniques as employed here proved an invaluable approach to obtain maximum information on the AdoMetDC inhibited proteome.

One of the proteins detected within this extreme pI range was histone H4 that was decreased in all of the bands. Another histone protein that was detected on the 1-DE gels and decreased in abundance was histone 2B. Histones form part of the nucleosome in eukaryotes and play an important role in chromatin packaging and structural organisation as well as regulation of all aspects of DNA function, which includes transcriptional control and DNA damage responses (Trelle *et al.*, 2009). The histone family consist of 4 histone classes that include H2A, H2B, H3 and

H4 which is regulated by PTM's that include acetylation, methylation, phosphorylation and ubiquitylation (Berger, 2002). These PTM's of the histones creates the "histone code" that may be recognised by transcription factors that will ultimately result in transcriptional responses (Strahl & Allis, 2000) or possible DNA repair (Wurtele & Verreault, 2006) and therefore epigenetic regulation and DNA metabolism control. The histone protein levels detected in the 1-DE AdoMetDC inhibited proteome does not reflect the histone PTM's and therefore only indicated protein abundances and not any type of PTM. Histones are in low abundance in ring and early trophozoite stages but increase in abundance in late trophozoite and schizont stages, which coincides with the parasite going through active DNA synthesis to prepare for schizogeny (Miao *et al.*, 2006). Since the AdoMetDC inhibited protein samples were harvested at 16 HPI and 20 HPI which is in the early trophozoite stages, it is therefore indicative of the sensitivity of the 1-DE coupled with LC-ESI/MS approach which were able to detect proteins that were in low abundance.

Various polyamine specific-proteins were identified within the AdoMetDC inhibited proteome. The protein levels of pyrroline-5-carboxylate reductase (MAL13P1.284) were increased in abundance with AdoMetDC inhibition, while the protein levels of eIF5A (PFL0210c) were decreased in abundance. The increased protein abundance of pyrroline-5-carboxylate reductase (MAL13P1.284) may be as an attempt to utilise L-glutamate-5-semialdehyde for conversion to proline. Closely linked to pyrroline-5-carboxylate reductase (MAL13P1.284) is OAT which is able to catalyse the reversible reaction from L-glutamate-5-semialdehyde into ornithine. Therefore, the regulation of OAT protein abundance may play a role on pyrroline-5-carboxylate reductase (MAL13P1.284) through the regulation of L-glutamate-5-semialdehyde and ornithine. The protein abundance of OAT remained unchanged in Tt_1 and could not be determined in Tt_2 due to the spots of OAT and AdoMet synthase that overlapped on the 2-DE gels. Therefore, the increase in abundance of pyrroline-5-carboxylate reductase (MAL13P1.284) remains unclear, and prompts further investigation into the metabolite levels within this pathway to elucidate the reason for increased protein abundance of pyrroline-5-carboxylate reductase (MAL13P1.284).

The protein abundance of eIF5A was decreased. Although putrescine is formed by ODC with the inhibition of AdoMetDC, its conversion to spermidine is prevented (Das Gupta *et al.*, 2005). The synthesis of eIF5A is dependent on the production of spermidine (Park *et al.*, 1981) and the decreased protein abundance of eIF5A may therefore be as a result of spermidine depletion due to AdoMetDC inhibition. Decreased expression of eIF5A may result in decreased protein synthesis for the parasite. The decreased protein abundance of eIF5A is similar to previous results which were obtained by the inhibition of *Pf*AdoMetDC with SAM486A (Blavid *et al.*, 2010). eIF5A is a unique

small acidic protein and is the only protein that contains the unique amino acid hypusine [N^{ε}-(4-amino-2-hydroxybutyl)lysine] (Park *et al.*, 1991, Park *et al.*, 1997). The spermidine dependent biosynthesis of hypusine in eIF5A is the most specific post-translational modification to date of which eIF5A hypusinylation is essential for eukaryotic cell proliferation (Park, 2006, Cooper *et al.*, 1982) and translational initiation for protein synthesis (Park *et al.*, 1991, Wolff *et al.*, 2007, Molitor *et al.*, 2004, Park, 2006).

Previously, cytostasis has been observed in spermidine-deprived L1210 cells after the inhibition of AdoMetDC and the cytostasis was attributed to the depletion of the hypusine-containing eIF5A (Byers *et al.*, 1994). Similarly, in human colon cancer cells polyamine-depletion also resulted in a cytostatic effect which was attributed to a decrease in protein synthesis as a result of decreased protein expression of eIF5A (Ignatenko *et al.*, 2009). eIF5A is transcribed throughout the *P. falciparum* lifecycle (Molitor *et al.*, 2004, Le Roch *et al.*, 2004, Bozdech *et al.*, 2003), emphasising the importance of this protein in the developmental stages of the malaria parasite (Kaiser *et al.*, 2007) and its involvement in cell proliferation within the parasite (Kaiser *et al.*, 2007, Kaiser *et al.*, 2003b, Kaiser *et al.*, 2003a). Therefore, eIF5A synthesis is dependent on spermidine levels, but it should be noted that only eIF5A protein abundance levels were determined within the AdoMetDC inhibited proteome and the protein abundance does not necessarily determine the hypusinilation of eIF5A which will determine the function of the eIF5A protein. Previous evidence suggests that AdoMetDC inhibition and subsequent spermidine depletion may result in decreased protein abundance of the functional eIF5A protein (Blavid *et al.*, 2010).

Other polyamine-related proteins that were identified during the 2-DE proteomic investigation of inhibited *Pf*AdoMetDC included PNP (PFE0660c), adenosine deaminase (PF10_0289), AdoMet synthase (PFI1090w) and PEMT (MAL13P1.214). The protein abundance of AdoMet synthase was decreased in Tt_1. Two protein isoforms was identified for PNP of which 1 was decreased and the other increased in abundance. Three protein isoforms was identified for PEMT of which 2 were decreased and 1 increased in abundance. Upon validation of the PEMT protein levels with 2-D immunoblotting it was determined that at least 4 protein isoforms exist for PEMT of which all of them had decreased protein expression. The western blot for PEMT was conducted on a 13 IPG strip while the 2-DE gels were performed using 18 cm IPG strips. It is therefore possible that even more isoforms do exist, since the 2-DE gels reveal a cluster of at least 6 protein spots in the range of PEMT that may all be PTM's of PEMT. More than 500 protein PTM's have been discovered, with new ones being added regularly as the technology improves (Krishna & Wold, 1993). The importance of PTM's has recently been demonstrated by the detection of several isoforms that have

differential expression (Nair *et al.*, 2008), which may also be the case for PEMT and PNP in the AdoMetDC inhibited proteome. Few regulatory motifs and transcription regulators have been uncovered in Plasmodial parasites (Coulson *et al.*, 2004) and since transcription within the parasite may be hard-wired (Ganesan *et al.*, 2008) it may suggest that post-transcriptional and post-translational mechanisms are regulating the parasite life cycle as well as have a role in invasion and egress (Chung *et al.*, 2009).

Several heat shock proteins were detected at both time points that included heat shock protein 70 (PF08_0054) that had increased protein abundance in both time points, while heat shock protein 86 (PF07_0029) and heat shock protein 60 (PF10_0153) had decreased protein levels at Tt_1. Heat shock proteins are encountered throughout the erythrocytic life stages of the parasite and can act as chaperones as well as enable the parasite to survive temperature fluctuations often associated with malarial infections (Misra & Ramachandran, 2009). Heat shock protein 70 (PF08_0054) has also been implicated in the transport of nuclear encoded proteins to the apicoplast (Foth *et al.*, 2003). It is therefore not surprising, that upon inhibition of AdoMetDC, the protein abundances of heat shock proteins 70 (PF08_0054) and 60 (PF10_0153) were increased over time from Tt_1 to Tt_2 to help the parasite cope with increased stress.

The protein abundance of actin-1 (PFL2215w) was decreased at Tt_2. In *Trichomonas vaginalis* a 2-DE approach determined that actin-1 consisted of 8 different isoforms which may enable the rapid changes in morphology associated with the parasite (De Jesus *et al.*, 2007). Recently, it has been determined in HeLa cells that polyamines are essential for microtubule formation, and as a consequence polyamine depletion would result in decreased microtubule formation (Savarin *et al.*, 2010). The results obtained with the AdoMetDC inhibited proteome therefore provide evidence that spermidine and spermine depletion as a result of AdoMetDC inhibition within Plasmodial parasites may also hinder microtubule formation.

The protein abundances of leucine aminopeptidase (PF14_0439) and 3 isoforms of the M1-family aminopeptidase (MAL13P1.56) were increased, while HAP protein (PF14_0078), plasmepsin-2 (PF14_0077) and 2 isoforms of falcipain-2 (PF11_0165) had decreased abundances. Elongation factor 2 (PF14_0486) was detected as 3 isoforms of which the protein abundance of 2 isoforms increased, while the other protein isoform had decreased protein abundance. All these proteins play a role in translation and protein synthesis either by providing amino acids from hemoglobin degradation for translation or by initiation of translation. Therefore the AdoMetDC inhibition is able to differentially affect proteins associated with protease activity as well as translation.

Various glycolytic proteins were identified at both time points and had both increased and decreased protein abundance. Hexokinase (PFF1155w) was either at undetectable protein levels or completely absent in the treated samples. The protein levels of phosphoglycerate kinase (PFI1105w) and glyceraldehyde-3-phosphate dehydrogenase (PF14_0598) was decreased in abundance, while pyruvate kinase (PFF1300w) consisted of various isoforms of which 1 had increased protein abundance and 1 had decreased protein abundance. Phosphoglycerate kinase (PFI1105w) and pyruvate kinase (PFF1300w) are the only enzymes able to produce ATP to provide energy during glycolysis (Roth *et al.*, 1988a). $NADP^+$-dependent glutamate dehydrogenase (GDH; PF14_0164) was detected as 3 isoforms. Two of these isoforms were increased in abundance at both Tt_1 and Tt_2, while the other isoform were decreased in abundance at both time points. GDH is present within all the stages of the intraerythrocytic life cycle of the parasite and is the major source of NADPH (Roth, 1990, Wagner *et al.*, 1998). Glycolysis is integral to parasite survival since the parasite relies on a constant supply of glucose and subsequently also imports large quantities of glucose into the erythrocyte for parasite utilisation (Saliba *et al.*, 2003). As a consequence of the large glucose utilisation of the parasite most of the glycolytic enzymes within the parasite are elevated to ensure that the energy needs of the parasite are met (Roth *et al.*, 1988b). Therefore, the AdoMetDC inhibited proteome revealed differential regulation of various isoforms of the glycolytic pathway, although the PTM's associated with the various isoforms needs further investigation to elucidate the functional state of the specific proteins.

T. brucei, T. cruzi and *Leishmania* does not contain catalase (Flohe *et al.*, 1999). *P. falciparum* is also devoid of catalase. The parasite is able to take up the human Cu/Zn SOD from its host to help with detoxification (Fairfield *et al.*, 1983 (b), Fairfield *et al.*, 1983 (a), Fairfield & Meshnick, 1984). Recently it has also been shown that human peroxiredoxin-2 is imported into the parasite cytosol and accounts for 50% of the overall thioredoxin peroxidase activity within the parasite (Koncarevic *et al.*, 2009). Once taken up into the parasite the human peroxiredoxin-2 was detected as 6 protein isoforms in all the intra-erythrocytic life stages of the parasite. CQ drug pressure of the parasites resulted in increased import of the human peroxiredoxin-2 to alleviate oxidative damage (Koncarevic et al., 2009). Previous drug perturbation proteomic studies also detected human peroxiredoxin-2, but it was considered as human contaminating proteins (Makanga et al., 2005, Gelhaus *et al.*, 2005). In the AdoMetDC inhibited proteome both human peroxiredoxin-2 and human Cu/Zn superoxide dismutase were identified by MS and both proteins had decreased protein abundance at Tt_1. Therefore, the decreased protein abundances of the 2 human proteins with AdoMetDC inhibition may be as a result of decreased import of the human proteins into the parasite

in an attempt to preserve energy. The decreased protein abundances of these 2 human proteins may therefore also result in a state of increased oxidative stress within the parasite.

The parasite is heavily dependent on an efficient detoxification system, since both the parasite and the host erythrocyte is under constant oxidative stress due to the presence of oxygen and iron (Muller, 2004). The protein abundance of GST (PF14_0187) was decreased at Tt_1, but increased in protein abundance at Tt_2. The parasite has only one copy of the GST gene (Srivastava *et al.*, 1999) and inhibition of GST would disturb the GSH-dependent processes within the parasite resulting in an increase in the concentration of FPP IX produced during hemoglobin digestion and hence enhanced cytotoxic levels (Deponte & Becker, 2005, Hiller *et al.*, 2006). The trend of increased protein abundance of GST over time may suggest an attempt by the parasite to detoxify toxic metabolites.

2-Cys peroxiredoxin (PF14_0368) was detected in the AdoMetDC inhibited proteome, with the protein abundance of this protein progressively increasing over the 2 time points. 2-Cys peroxiredoxin and 1-Cys peroxiredoxin form part of the thioredoxin superfamily proteins necessary for detoxification that include thioredoxin, glutaredoxin and plasmoredoxin of which plasmoredoxin is unique to Plasmodial parasites (Becker *et al.*, 2003). An increase in the abundances of both the transcript and protein of 2-Cys peroxiredoxin has been reported which was associated with increased oxidative stress within the parasite (Akerman & Muller, 2003). Therefore, the increased protein abundance of 2-Cys peroxiredoxin within the AdoMetDC inhibited proteome may be an attempt by the parasite to cope with the increased oxidative stress within the parasite.

From the AdoMetDC inhibited proteome data obtained at the 2 time points investigated it is proposed that the inhibition of AdoMetDC results in decreased hemoglobin digestion, decreased microtubule formation, differential regulation of glycolytic enzymes and regulation of the redox status of the parasite. The AdoMetDC inhibited proteome is therefore dynamic and able to respond to drug pressure exerted by MDL73811.

In the next chapter, the AdoMetDC inhibited transcriptome will be investigated. Even with the improved 2-DE applied here to the AdoMetDC inhibited proteome only 119 protein spots could be determined that were differentially affected. Therefore, the proteomic study for AdoMetDC inhibition remained limited to soluble proteins within the pI range of 3-10 and molecular weight of 15 to 120 kDa. In an attempt to obtain a more global view and a larger dataset the transcriptome will be investigated with the hope of finding more differentially affected transcripts.